Research Square

Preprints are preliminary reports that have not undergone peer review.
They should not be considered conclusive, used to inform clinical practice,
or referenced by the media as validated information.

Effective Catalytic Esterification of Fat-Oil-Grease into Biodiesel over Sulfonated Zinc-Carbon Catalysts

M. Vasanthan
National University of Malaysia
G. Abdulkareem-Alsultan
kreem.alsultan@yahoo.com
Universiti Putra Malaysia
N. Asma-Samsudin
National University of Malaysia
S. Mohd Yusof
National University of Malaysia
Siti Aishah Hasbullah
National University of Malaysia
Y. H. Taufiq-Yap
Universiti Putra Malaysia
Rahimi Yusuf
National University of Malaysia
Koici Ichimura
Hokkaido University
Isou Watanabe
RIKEN Center for Sustainable Resource Science
Ambar Yarmo
National University of Malaysia
I. Nur Azreena
Malaysian Palm Oil Board
M. Hasif Auji
National University of Malaysia
Stella Jovita
Sepuluh Nopember Institute of Technology
Didik Prasetyoko
Sepuluh Nopember Institute of Technology
B. Hazmi

Universiti Putra Malaysia

Siti Sarahah Sulhadi

Universiti Putra Malaysia

N. Asikin-Mijan

National University of Malaysia

Research Article

Keywords: Activated carbon, biodiesel, esterification, sulfonation, Zinc

Posted Date: September 1st, 2026

DOI: https://doi.org/10.21203/rs.3.rs-10787952/v1

License: This work is licensed under a Creative Commons Attribution 4.0 International License.
Read Full License

Additional Declarations: No competing interests reported.

Effective Catalytic Esterification of Fat-Oil-Grease into Biodiesel over Sulfonated Zinc-Carbon Catalysts

Highlights

I. Zn-sulfonated carbon catalyst derived from sunflower husk via hydrothermal carbonization.
II. Exhibited high fat oil grease esterification due to abundant acid sites and strong Zn-S bonding.
III. Achieved 81% conversion and 98% biodiesel yield at 70 °C, 120 min, and 20:1 MeOH:oil ratio using 3 wt% catalyst.
IV. Strong Zn-S interaction ensured excellent reusability over 4 cycles.

Abstract

This study investigates the synthesis of sulfonated-zinc carbon catalysts (ACZnS-220-5wt%). All catalysts were prepared via carbonization using hydrothermal treatment of sunflower husk, followed Zn incorporation and sulfonation. The Zn-S promoted catalyst exhibited superior activity, achieving 81% fat-oil-grease (FOG) conversion, attributed to its higher surface area (~287 m^2/g) and high density of strong acid sites (~3855 μmol/g). XPS revealed presence of Zn,S and confirmed sulfur bonding enhanced by Zn addition and maximized through Zn,S coordination. 220°C hydrothermal treatment on sunflower husk during C conversion recombined with optimize Zn loading (5wt.%) exhibited superior esterification of FOG due to high existence of high surface area. Based on parametric study, an optimized ACZnS-220-5wt% catalyst achieved a 88% FAME yield under 3 wt% catalyst loading, 20:1 MeOH:oil ratio at 70 °C within 2 h. The catalyst efficiency was found stable up to 5^{th} cycles, confirming that the

strong Zn-S interaction contributes to its excellent reusability. The results highlight ACZnS-220-5wt% as an efficient, and sustainable heterogeneous catalyst for biodiesel production from waste FOG.

Keywords: Activated carbon, biodiesel, esterification, sulfonation, Zinc

1. Introduction

The current global aspiration and trend is leaning towards renewable energy. Renewable energy as is something that has been popping up for decades and reasonable and remarkable findings have been discovered in converting energy in converting energy such as biomass into liquid biofuels including biodiesel and green diesel [11]. Biodiesel or fatty acid methyl ester (FAME) is a promising liquid biofuel owing to its biodegradability, low sulphur content, and compatibility with existing diesel engines. Biodiesel is produced from transesterification/esterification process with additional of catalyst and methanol [29] . Noted, based on scopus there are 62,290 papers published papers on biodiesel (Elsevier B.V. Available at: https://www.scopus.com (Accessed: 13 July 2026)). Although biodiesel has been extensively studied and partially commercialized, its large-scale adoption remains limited due to the high cost of feedstock, which can account for up to 75% of the total production [5]. Moreover, the commercialization of biodiesel using edible feedstocks such as palm oil, sunflower oil, and soybean oil has raised concerns over the “food versus fuel” debate [1]. Consequently, waste-based feedstocks have emerged as a promising and sustainable alternative to address both economic and ethical challenges.

FOG is a by-product of household and industrial waste rich in FFA and triglycerides, mainly originating from the disposal of fats and oils from restaurants and food industries. FOG is a by-product of domestic and industrial waste rich in FFA and triglycerides, mainly

originating from the disposal of fats and oils from restaurants and food industries. FOG is generated in large quantities globally (≈25–30 million tonnes/year) and in Malaysia (0.5–1 million tonnes/year), with a significant portion discharged into drainage systems (Ahmed.R et al., 2021) Accumulated FOG solidifies and forms blockages ("fatbergs"), leading to sewer overflow and urban flooding. Its anaerobic decomposition produces foul odors (e.g., H_2S), while leakage into water bodies reduces dissolved oxygen and harms aquatic life. In soil, FOG clogs pores, disrupts microbial activity, and reduces fertility, ultimately degrading environmental quality and ecosystems [2] .Indeed, utilization of FOG as biodiesel feedstock not only reduces environmental pollution but also decreases dependence on edible oils . Critical reviews by [1]. and [3] highlight both the environmental benefits and technical challenges of utilizing FOG, particularly in managing its composition and waste treatment implications. Research has further emphasized the importance of heterogeneous acid catalysts as promising alternatives to replace corrosive homogeneous acids, providing better reusability and environmental compatibility. Former study by [3] reported that the FOG comprised of majority FFA content (FFA > 15 %) . Noteworthy to mention, due to high FFA (FFA> 15wt%), hence, the FOG needs to be esterified using acid catalyst for biodiesel production. Notably, transesterification process is not an ideal solution for biodiesel production from FOG, since transesterification in will used the base catalysts and it will lead to saponification reaction leading soap formation [3] . Therefore, an esterification step using acid catalysts is the most ideal pathways from transformation of FOG into biodiesel.

Conventional homogeneous acid catalysts such as H_2SO_4 are effective for esterification of high FFA feedstock (FFA > 5%), nevertheless due to biodiesel and catalyst separation issue along with production of massive wastewater led to the application of heterogeneous acid catalysts such ACZnO [34], HTCS [16] and carbon-based catalyst ([28]; [8]) . Notably, among them, sulfonated carbon catalysts derived from biomass are particularly attractive due to their

high acidity and sustainable nature [33], [8]. Nevertheless, sulfur leaching and reduced reusability remain significant challenges [16]. According [16] although HTC-S catalyst shows high esterification performance (~92% FFA conversion and ~85% FAME yield), its long-term stability is limited due to sulfur leaching during repeated reactions. The loss of -SO_3H groups reduce the number of strong acidic sites, leading to catalyst deactivation. Even though regeneration using concentrated H_2SO_4 can temporarily restore these active sites and maintain >90% FFA conversion for two cycles, the issue originates from relatively weak S-C bonding within the sulfonated carbon framework. Therefore, future studies should focus on improving the stability of the S-C bond, for example by introducing metal species that can form stronger metal-sulfur interactions and better anchor the -SO_3H groups on the carbon surface, thereby reducing sulfur leaching and improving catalyst durability. Recent studies ([28]; [40]) demonstrated enhanced catalytic activity when bio-derived activated carbon is functionalized with sulfonic groups, while additional doping with metal oxides, such as Zn, further improves acidity, thermal stability, and reusability through synergistic effects. For example, Zn-doped activated carbon with sulfur coating has shown increased catalytic activity and surface area [17].Wet impregnation using ethanol has been widely applied as an effective preparation method for incorporating metal species onto carbon supports, ensuring uniform dispersion and improved catalytic properties. Collectively, these findings suggest that metal-doped sulfonated carbon catalysts, particularly Zn-based systems, offer significant potential for optimizing the esterification of FOG into biodiesel. Zinc loading primarily introduces strong Lewis acid active sites, which are essential for driving chemical processes like the simultaneous esterification and transesterification of acidic waste oils [5]. Texturally, the addition of zinc oxide (ZnO) onto carbon supports typically triggers a partial blockage of the internal porosity, leading to a sharp decline in the specific surface area and pore volume as the metal particles fill the channels [25]. However, concentrating ZnO on the external surface can form a fibrous coating that avoids

diffusion restrictions inside narrow pore channels, thereby increasing reaction conversion and significantly enhancing the catalytic performance of renewable carbon catalysts [28]. Furthermore, zinc loading provides a pseudo-capacitive effect through faradic redox reactions in electrochemical applications and acts as a synergetic promoter to increase the density of acid-base active sites. Despite these benefits, high loading levels may be susceptible to metal leaching into the reaction medium during cycles, though intentional acid-leaching is a recognized strategy for recovering lost surface area and porosity.

Taking into consideration the idea [39], sunflower husk biochar produced via controlled pyrolysis shows a well-developed porous structure with the presence of macro- and mesopores, which act as effective transport channels for reactants and facilitate access to active sites. Although the intrinsic BET surface area of raw sunflower husk biochar is moderate, its lignocellulosic structure and honeycomb-like carbon framework, as observed by SEM, provide a stable matrix that can be further enhanced through chemical activation and sulfonation. Sunflower biochar prepared via hydrothermal carbonization is expected to exhibit a surface area of 50-300 m^2/g, while the sulfonated and Zn-modified catalyst is anticipated to range between 200-500 m^2/g due to pore blocking by $-SO_3H$ groups and metal incorporation; however, mesoporosity and acid site density are more critical than absolute surface area for effective FFA esterification. The biochar also contains surface oxygenated functional groups (e.g., -OH and -COOH), which promote effective anchoring of $-SO_3H$ groups. In addition, sunflower seed husk is an abundant agricultural waste and aligns with sustainable development principles, making it a cost-effective and renewable alternative to conventional catalyst supports. These combined structural, chemical, and sustainability advantages justify the selection of sunflower seed husk as a promising support material for SO_3H-functionalized solid acid catalysts.

Based on aforementioned findings, hence, the present study aims to synthesize and evaluate ACZnS and catalysts derived from sunflower husk-based activated carbon via three steps process, hydrothermal carbonization-impregnation-sulfonation process. Effect of hydrothermal carbonization temperature will be investigated the most effect temperature yielding high carbon concentrations. The catalytic performance was evaluated for FOG esterification, and the best-performing catalyst (ACZnS) was further optimized using One Variable at A Time (OVAT). Finally, the reusability and structural stability of ACZnS is examined over multiple reaction cycles to demonstrate the role of Zn in enhancing the stability of Zn-S bonding and minimizing sulfur leaching.

2. Materials and methods

2.1 Materials

Sunflower husk biomass was obtained supermarket located at Bangi area, washed, and oven-dried at 105 °C. Zinc nitrate hexahydrate ($Zn(NO_3)_2 \cdot 6H_2O$) (98% Purity), and concentrated sulfuric acid (98% Purity) were purchased from Merck. Methanol (99.9% Purity) ethanol (99.9%) and Hexane (HLPC Grade) (99.7%) obtained from Sigma Aldrich served as the esterification reagent and solvent. Potassium hydroxide (KOH, analytical grade) and phenolphthalein indicator was used for acid value determination. The standard methyl esters for GC analysis, such as methyl heptadecanoate, methyl oleate, methyl linoleate, methyl palmitate, methyl myristate, and methyl stearate were purchased from Fluka, USA. FOG was collected from Indah Water Konsortium Sdn. Bhd. (IWK), filtered, and dried at 100 °C to remove moisture and dirt. Distilled water was used throughout all experimental procedure and Ph paper was used for catalyst washing. The properties, water and free fatty acid (FFA) contents in the FOG were represented in **Table 1**. As for FOG, the total acid number (TAN) was analyzed to be 215 mg KOH/g. This number highlights the prevalence of FFA with 107

weights % . Based on the methyl ester, the chemical composition of the FFA in FOG dominated by the palmitic acid, C16:0 (56%) followed by oleic acid, C18:1 (38%) and traces amount of myristic acid, C14:0; stearic acid, C18:0; linoleic acid C18:2, respectively.

Table 1. Properties of the employed FOG.

Properties	Norm	Value	
Moisture content (% wt.)	ASTM D6304	9.45±0.1	
Saponification value (mg KOH/g oil)	AOCS Tr 1a-64	201.43±1.17	
Free Fatty Acid FFA content (%)	AOCS Cd 3d-63	107±1	
Acid value (mg KOH/oil)	AOCS Cd 3d-63	215±1	
Molecular weight (g/mol^{-1})		835	
FOG Composition		Ester[a]	Fatty acid[b]
Myristic acid (C14:0)		2.03	-
Palmitc acid (C16:0)		55.78	65.26
Stearic acid (C18:0)		1.69	-
Oleic acid (C18:1)		37.95	32.19
Linoleic acid (C18:2)		2.58	-
Others[c]		-	2.55

[a] The esterified FOG is determined by GC-FID
[b] Raw FOG is determined by GC-MS
[c] Other compounds: Cyclononasiloxane, erythro-9,10-Dibromopentacosane, 2-Dodecylcyclohexanone, Palmitoyl chloride

2.2 Catalyst Synthesis

The catalyst from sunflower seed husk was synthesized using a five-step process: mechanical grinding followed by hydrothermal carbonization, ethanol impregnation, calcination and finally sulfonization. Initially, sunflower seed husk is washed and dried at 100 °C overnight and then were grind into a very fine powder using a mini milling machine 1250 g

multi-function disintegrator (220-240 V~, 3500 W, 50-60 Hz, no25,000 r/min) for 2 min (Fig. 1a) and is sieved using 1 mm sieve. The powdered sunflower seed husk directly undergoes hydrothermal carbonization at 200°C using autoclave reactor with 3.75 g of powdered sunflower seed husk mixed with 75 mL distillate water for 10 h. The treated powdered sunflower seed husk was filtered, washed with distilled water till pH = 7 at room temperature prior to drying at 100 °C for 12 h. The dried sample were later crushed to obtain fine powder and denoted as (biochar (BC)). 1.5g of BC was then impregnated with 6.83g zinc nitrate hexahydrate (50 wt.% Zn) using 90 mL ethanol under continuous stirring for until fully evaporated. The 1:1 Zn precursor-to-activated carbon ratio was selected as the initial preparation condition referencing [4]. The enhanced performance observed at a 1:1 ratio was attributed to synergistic interactions between the active Zn species and the supporting component, suggesting that a balanced formulation may promote effective Zn dispersion and interaction with the carbon matrix. The mixture was dried at 60 °C overnight and calcined at 550 °C for 3 h and denoted as ACZn-200-50 wt%. 2g of the compound was later further treated with 100 mL of sulfuric acid under reflux system at 150 °C for 8 h. The slurry is filtered and washed with hot distillate water (80 °C) till pH = 7 to remove unreacted sulfuric acid and dried for 1 h at 100 °C. The obtained powder was denoted as ACZnS-200-50wt%. Same procedures were repeated on Zinc AC but without the presence of sulfur which denoted as ACZn-200-50wt%.

2.3 Catalytic optimization

Optimization of catalyst tests were done by varied the hydrothermal carbonization temperature (HTC) (180 °C, 200 °C, 220 °C and 240 °C) and Zinc loading (1wt%, 5wt%,10wt%,15wt% and 20wt%). The details on the parameter are listed in Table 2. Each catalyst parameter was optimized via *One Variable At a Time (OVAT)*. The optimized reaction

parameters were also determined using OVAT method. OVAT method is when a single reaction parameter was varied while the remaining parameters were kept constant to evaluate their individual effect on biodiesel yield. The parameters investigated for reaction parameters were in the following order, reaction temperature (60°C , 70°C , 80°C and 100 °C), methanol to oil ratio (1:10, 1:14, 1:20 and 1:25), reaction time (1h, 2h, 3h and 5h), and catalyst loading (1 wt%, 3wt%, 5wt% and 7wt%). Each parameter was studied sequentially to determine the optimum operating conditions for the esterification reaction. After determining the optimum reaction condition reusability test was carried out. The reusability of catalyst is crucial in making the catalyst economically effective and industrially ready. In reusability study, each cycle the spent catalyst was washed with methanol, dried at 110 °C, and reused. optimized catalyst was tested for five cycles under optimal conditions. The esterification activity further confirmed by FFA conversion.

Table *2*. Optimization parameters and catalyst designation

Optimization Parameter	**Parameter condition (catalyst designation)**
Hydrothermal temperature	180 °C (ACZnS-180-50wt%)
	200 °C (ACZnS-200-50wt%)
	220 °C (ACZnS-220-50wt%)
	240 °C (ACZnS-240-50wt%)
Zinc loading	1wt% (ACZnS-220-1wt%)
	5wt% (ACZnS-220-5wt%)
	10wt% (ACZnS-220-10wt%)
	15wt% (ACZnS-220-15wt%)
	20wt% (ACZnS-220-20wt%)

204 *2.4 Esterification test of FOG*

205 The esterification reaction was carried out in a 150 mL two-neck round-bottom flask
206 equipped with a reflux condenser and a magnetic stirrer. Approximately 10 g of FOG with
207 properties shown in **Table 1**, 0.3 g of the synthesized catalyst (ACZn-200-50wt%, ACZnS-200-
208 50wt%.), and 6.8 mL of methanol were mixed and refluxed at 70 °C in an oil bath for 2 h under
209 vigorous stirring [16]. The resulting solution was then centrifuged to separate the solid catalyst
210 from the methanol-biodiesel mixture. The product was subsequently heated at 70 °C for 1 h.
211 The acid value for the biodiesel was determined followed by FFA% conversion.

212

213 *2.5 Catalyst Characterization*

214 The elemental composition of fresh Biochar and raw sample was analyzed using a CHNS/O
215 analyzer (TruSpec, LECO) to determine total amount of carbon, hydrogen, nitrogen, sulfur, and
216 oxygen in the sample. An X-ray diffractometer (XRD; Model XRD 6000, Shimadzu) was used
217 to study the structures of the synthesized samples. The instrument employed Cu-Kα radiation
218 ($\lambda = 0.15406$ nm) at 30 kV and 15 mA, and scans were conducted over the 2θ range of 10°-80°
219 with a scanning rate of 2° min^{-1}. The Brunauer-Emmet-Teller (BET) model was used to
220 determine the surface area and pore distribution of the catalysts with a Sorptomatic 1990 series
221 instrument (Thermo Finnigan). Pore diameter distributions were determined by the Barrett-
222 Joyner-Halenda technique from the desorption loop. The functional groups of the catalyst were
223 studied by using Fourier transform infrared (FTIR) spectroscopy with a Perkin Elmer 1650
224 spectrometer; peaks were recorded in the range of 400-4000 cm^{-1}. Temperature-programmed
225 desorption of ammonia (TPD-NH_3) was used to identify the total acidity of catalysts that had
226 been pre-treated under a N_2 environment to remove moisture and impurities. The pre-treated
227 catalysts were saturated with NH_3 for 1 h and then flushed with N_2 at a rate of 30 $mLmin^{-1}$ The
228 N_2-absorbing catalysts were heated from 50 °C to 900 °C, and the desorbed gas was interpreted

by using a TPD/R/O 1100 instrument (Thermo Finnigan). Field-emission scanning electron microscopy (FESEM; JEOL JSM7600F) was used to examine the morphology of the catalysts. The elemental composition of fresh catalysts was also further determined by field emission scanning electron microscopy (FESEM) fitted with EDX analysis using Rayny EDX-720 spectrometer and Jeol JSM-7600F. X-ray photoelectron spectroscopy (XPS) was employed to determine the surface elemental composition and oxidation states of the catalysts. Measurements were conducted under ultra-high vacuum conditions using monochromatic Al Kα radiation, and spectra were calibrated using the C 1s peak.

2.6 Product analysis

The acid value (AV) of FOG and biodiesel was determined according to the AOAC Cd 3d-63 standard Eq.1. The FFA conversion of the collected products was determined using the European standard method EN 14103, as shown in Eq. 2. The biodiesel or fatty acid methyl ester (FAME) yield was calculated based on the European standard EN 14103 using Eqs. 3-5. An example of GC-FID calculations is presented in the calculation excerpt. The response factor (RF) for each compound was calculated using a standard compound (methyl heptadecanoate) according to Eq. 3. Subsequently, the FAME content was calculated using Eq. 4, and the FAME yield (%) was determined using Eq. 5.

$$\text{Acid value (AV)} = \frac{A \times N \times X}{W} \qquad \text{(Eq. 1)}$$

Where A represents the volume (mL) of H_2SO_4 used, N is the normality of H_2SO_4, X (g/mol) is the molar mass of H_2SO_4, and is the mass of the sample (g).

$$\text{FFA conversion (\%)} = \frac{AV_f - AV_p}{AV_f} \qquad \text{(Eq. 2)}$$

where AV_f and AV_p represent the acid values of the feedstock and product, respectively.

$$RF = \frac{A_{IS} \times C_{rs}}{A_{rs} \times C_{IS}} \quad \text{(Eq. 3)}$$

where $A_{IS}$is the internal standard peak area, A_{if} is the internal standard concentration, RF is the reference standard peak area, and A_{iSS} is the reference standard concentration. The reference standard RF value was applied to all samples to calculate the FAME yield (%).

$$\text{FAME} = \frac{C_{iSS} \times A_{if} \times RF}{A_{iSS}} \quad \text{(Eq. 4)}$$

where A_{iSS} is the internal standard concentration in the sample, A_{if} is the internal standard peak area in the sample RF, and is the peak area of an individual FAME compound in the sample.

$$\text{FAME yield (\%)} = \frac{\text{mass of FAME in the product calculated by GC (g)}}{\text{mass of collected FAME (g)}} \text{(Equation 5)}$$

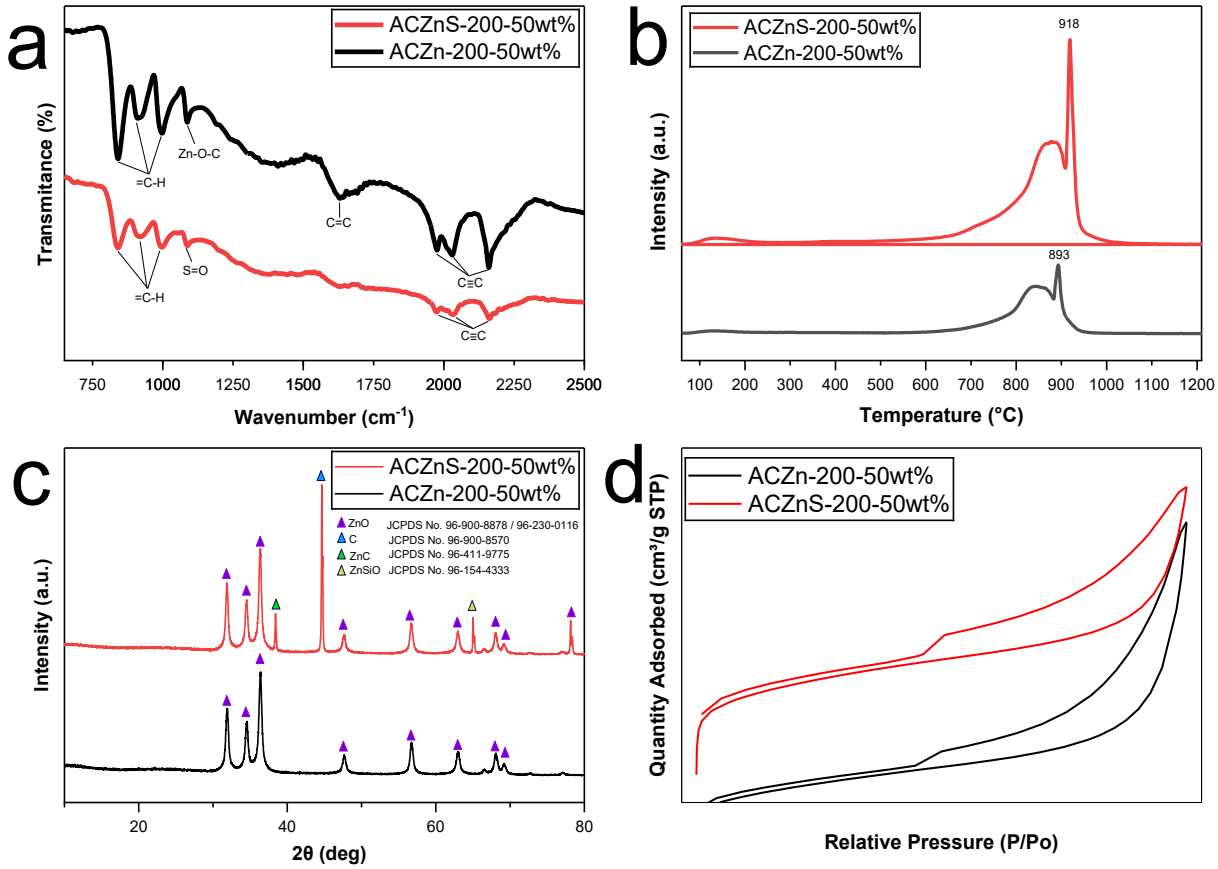
3. Result and discussion

3.1 Preliminary esterification study of FOG catalysed by ACZn and ACZnS

Referring to our previous group study [16], which used sulphated and non-sulphated AC derived from corn-cub to esterify PFAD into biodiesel shows that AC sulphated catalyst gives superior activity 92% of FFA conversion and 85% biodiesel conversion. Although the fresh catalyst exhibited promising esterification activity, its practical applicability was limited by poor stability, as it could only be reused for a single reaction cycle due to significant sulfur leaching. To address this limitation, the present study incorporated Zn species to strengthen the interaction between sulfur species and the AC support, thereby mitigating sulfur loss during the reaction. The esterification performance of the resulting Zn-modified catalyst (ACZn-200-50wt%, ACZnS-200-50wt%) were subsequently evaluated using FOG as the feedstock. Prior

274 the reaction, the catalyst with and without S species were characterized by FTIR, XRD, TPD-
275 NH_3, BET, and FESEM and the result showed in Fig. 1(a-d). The successful incorporation of
276 sulfur species was verified by FTIR analysis, which showed a characteristic S=O band at 1089
277 cm^{-1} for ACZnS-200-50wt%. The presence of sulfur species significantly increased the density
278 of strong acid sites, yielding a total strong acidity of 4098.5 μmol g^{-1}. Consequently, the catalyst
279 exhibited enhanced activity toward the esterification of high-FFA feedstocks. Notably, sulfur
280 addition increased the total acid density by 10.83%, further confirming that sulfur species are
281 the main contributors to the catalyst's acidity, which can facilitate adsorption and activation of
282 reactants, thereby promote esterification reaction. Distinct peaks observed at approximately 2θ
283 = 31.4°, 34.4°, 36.2°, 47.5°, 56.8°, and 62.8° belong to hexagonal zinc oxide (ZnO) with the
284 wurtzite crystal structure (space group $P6_3mc$) [JCPDS No. 96-900-8878] and 78.14° for ZnO
285 with high-angle reflections of hexagonal (ref) [JCPDS No. 96-230-0116] while 44.7° [JCPDS
286 No. 96-900-8570] belong to graphite. Indeed, the catalyst also showed minor reflections at the
287 existence at 38.4° and 65.0° belong to secondary phases [ZnC, ZnSiO] [JCPDS No. 96-411-
288 9775] [JCPDS No. 96-154-4333], respectively. These reflections suggest the possible
289 formation of secondary zinc-containing phases during catalyst synthesis. BET analysis revealed
290 that ACZnS-200-50wt% possesses a relatively low surface area (~9 m^2/g) compared to ACZn-
291 200-50wt% (~24m^2/g). Additionally, all catalysts exhibited Type IV isotherms, confirming
292 mixture of mesoporous and microporous structure, which is particularly advantageous for
293 esterification of FOG as it allows diffusion of bulky FFA molecules into the mesoporous
294 catalyst pores [14]. The introduction of sulfur species led to partial obstruction of the pore
295 network, as evidenced by the 70.8% and 22.1% reduction in pore volume and pore diameter
296 relative to ACZn-200-50wt%. Consequently, a decrease in BET surface area was observed,
297 which can be attributed to the deposition of sulfur-containing species within the catalyst pores,
298 thereby limiting pore accessibility [26]. Interestingly, FESEM analysis revealed that ACZnS-

200-50wt% exhibited a less porous structure (See Fig. 2(b) and (d)), which is expected to promote sulfur anchoring and enhance the exposure of catalytically active sites. Based on primilinary study on esterification of FOG using non-sulfated and sulfated Zn-modified catalyst (Fig. SX). Sulfonated catalysts exhibited significantly enhanced activity, with ACZnS-200-50wt% achieving the highest FFA conversion (~73.4%), followed by the non-sulfonated catalysts ACZn-200-50wt% (~9.4%) which showed poor performance. The superior catalytic activity of ACZnS-200-50wt% is attributed to its high density of strong acid sites, as confirmed by NH_3-TPD analysis. Interestingly, despite its lower surface area and smaller pore size, ACZnS-200-50wt% exhibited enhanced esterification performance, suggesting that catalytic activity is primarily governed by strong acidic sites rather than textural properties. This finding indicates that the reaction predominantly occurs on the external surface of the catalyst [33]. Overall, the superior catalytic activity of ACZnS-200-50wt% can be attributed to a combination of factors such as higher density and strength of acid sites from -S groups and strong bond strength between Zn and S.



313

314 **Figures 1.** (a) FTIR analysis for ACZnS-200-50wt% and ACZnS-200-50wt% (b) TPD-NH_3

315 analysis for ACZn-200-50wt% and ACZnS-200-50wt% % (c) XRD analysis for ACZn-200-

316 50wt% and ACZnS-200-50wt% (d) BET analysis for ACZn-200-50wt%, ACZnS-200-50wt

317

318 *3.2 Catalytic optimization study*

319 *3.2.1 Optimization of hydrothermal treatment*

320 The HTC process is a critical step that determines the physicochemical characteristics

321 of the carbon support, including its porosity, surface functionality, and structural integrity [27].

322 The formation of biochar was further validated through mass determination from 3.75 g of

323 powdered sunflower seed husk. At the optimal temperature of 220 °C, a balance is achieved

324 between carbonization and functional group preservation which is the main finding from

325 (**Table 2**) [38], who reported that hydrochar produced at 220 °C exhibited the highest oxidation

resistance. Noted, high HTC temperature (240°C) exhibit less mass of BC, which can be attributed to primary decomposition or secondary decomposition of the solid residue at higher temperature as mentioned by [35] and further states that the BC obtained had the heating value almost equivalent to coal a low−grade carbon (ratio H/C <1) (Table 3)). Noted, CHNS analysis also confirmed that the H/C atomic ratio decreased with increasing HTC temperature, indicating enhanced aromatization and carbonization of the hydrochar, consistent with the findings of [10]. Although a lower H/C ratio is associated with improved structural stability, excessive carbonization may reduce the abundance of surface functional groups. Overall, 220 °C was identified as the optimal HTC temperature for sunflower seed husk, providing a favorable balance between carbonization and material preservation, as evidenced by lower mass loss and an appropriate H/C ratio. Therefore, 220 °C was selected as the optimum HTC temperature for BC production for all Zn-modified catalysts.

Table 3. CHNS elemental analysis for Biochar

Hydrothermal temperature(°C)	Mass of BC	Element wt%				H/C ratio[a]
		Carbon	Hydrogen	Nitrogen	Sulphur	
Raw	-	44.28	6.67	0.21	-	1.79
180	2.34	49.67	6.66	0.00	-	1.59
200	2.14	53.58	6.70	0.30	-	1.49
220	1.79	60.32	6.37	0.44	-	1.26
240	1.35	70.37	5.90	0.65	-	1.00

a: Determined by (H/Molar Mass H) / (C/ Molar Mass)

3.2.2 Catalytic characterization

XRD analysis was performed to identify the changes in crystalline phases. Indeed, the raw biochar exhibits a broad diffraction peak centered around 2θ ≈ 20-30°, which is

characteristic of lack of long-range crystalline order owing by amorphous carbon (Fig. 2 a)[15]. Upon chemical modification and metal incorporation, there are visible changes in the diffraction patterns that were observed. The modified samples (ACZN (Fig 2 b) and ACZNS (Fig. 2 c)) display additional diffraction peaks, indicating the formation of crystalline phases on the biochar surface. Distinct peaks observed at approximately $2\theta = 31.4°$, 34.4°, 36.2°, 47.5°, 56.8°, and 62.8° [JCPDS No. 96-210-1125] can be attributed to wurzite ZnO, confirming the successful incorporation of zinc species into the catalyst structure. The presence of ZnO peaks suggests that zinc is present in a crystalline form rather than being completely amorphous or highly dispersed. Additionally, peaks corresponding to hexagonal carbon structure carbon [JCPDS No. 96-900-8878] (C) were observed at approximately $2\theta = 22.37°$. The persistence of these peaks in both raw and modified samples indicate that carbon remains structurally stable throughout the modification process [15]. Despite the appearance of crystalline peaks, the broad amorphous carbon peak remains visible in all samples, suggesting that the fundamental carbon structure is preserved after modification. In contrast, the sulfonated catalyst (ACZNS) does not exhibit distinct ZnO diffraction peaks, indicating a loss of crystallinity after sulfonation due to acid treatment, this finding also strongly supported by [22]'s finding, whereby using Sodium sulphide with ZnO showed similar anomaly of sulfide is added to the system an additional phase appears as the peaks characteristic to the zincite phase disappear. The effects of sulphonization on ZnO is more evident in research by Barnerjee and Jain findings where increase in sulphonization decreases the intensity of ZnO phase [7] . Overall, the XRD results confirm that the modification process successfully introduced crystalline ZnO phases in ACZN, while subsequent sulfonation in ACZNS leads to the transformation of Zn species into a more dispersed, amorphous state without compromising the carbon framework.

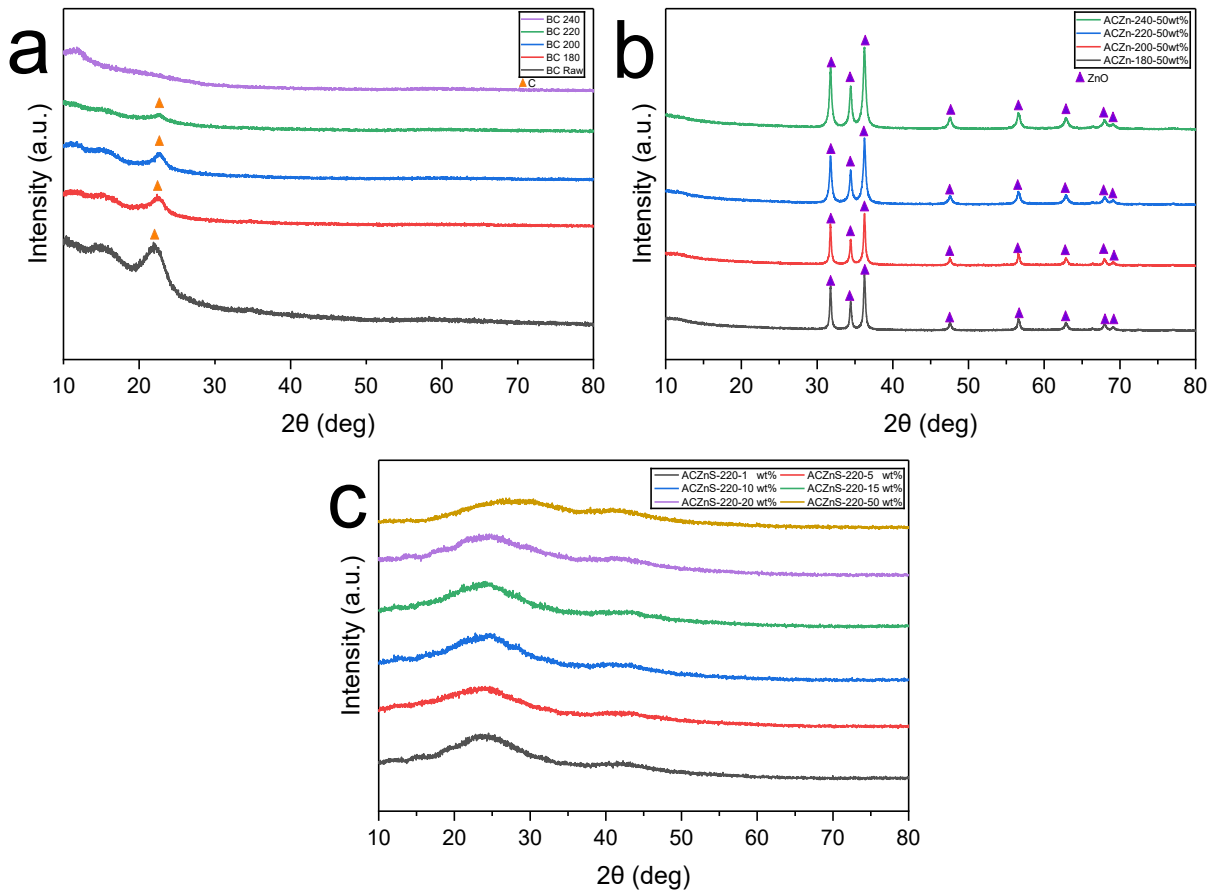


Figure 2. (a) XRD analysis for Raw-BC, BC-180, BC-200, BC-220 and BC-240 (b) XRD analysis for ACZn-180-50wt%, ACZn-200-50wt%, ACZn-220-50wt%, and ACZnS-240-50wt% (c) XRD analysis for ACZnS-220-1wt%, ACZnS-220-5wt%, ACZnS-220-10wt%, ACZnS-220-15wt%, ACZnS-220-20wt%, ACZnS-220-50wt%

BET surface morphology analysis revealed significant changes in the textural properties of the catalysts following sulfonation and variation in Zn loading, as summarized in **Table 4**. The unsulphated ACZn-220-50wt% catalyst exhibited the lower BET surface area of 104.11 m^2/g with a pore diameter of 6.17 nm and pore volume of 0.16 cm^3/g. While the BET surface area for ACZnS-220-1wt% showed lowest surface area of 8.45 $m^2\ g^{-1}$and pore volume 0.007 indicating the increase of Zn loading supports the structural integrity of catalyst as 5% Zn there is a sharp increase in surface area. Following sulfonation, the ACZnS catalysts demonstrated a substantial enhancement in surface area and porosity, indicating the development of a more

porous carbon framework. The BET surface area increased progressively from 287.53 m^2/g for ACZnS-220-5wt% to 600.70 m^2/g for ACZnS-220-50wt% . Similarly, pore volume increased from 0.18 cm^3/g to 0.64 cm^3/g with increasing Zn loading. This trend suggests that the incorporation of Zn species during synthesis promoted pore development and prevented excessive pore collapse during thermal treatment [18]. The increase in pore volume further indicates the formation of additional accessible pores within the carbon matrix [41]. All catalysts except ACZnS-220-1wt% display Type IV adsorption-desorption isotherms with distinct H1 and H4 hysteresis loops, confirming the presence of combined micro-mesoporous structures. As for ACZnS-220-1wt%, it shows Type II isotherm with an H3 hysteresis loop indicates that the 1 wt% catalyst is essentially non- or weakly porous/macroporous with slit-shaped pores formed by particle aggregation, unlike the higher Zn-loaded catalysts. The hysteresis H1 and H4 loops indicate capillary condensation within mesopores, which is consistent with the pore diameter values reported in **Table 4** (2.03-4.26 nm), demonstrating that all ACZnS catalysts possess mesoporous characteristics suitable for FFA diffusion during esterification. Indeed, low Zn loading result is smaller pore diameter while rich Zn loading cause enlargement of pore diameter, this is attributed to dehydration, dehydrogenation, deoxygenation and aromatization reactions by the sulphuric acid which is similar to Li's findings which involves $ZnCl_2$ to AC [20]. Notably, ZnO is proven to retain microporous structures [41] which is evident with the near similar microporous structures seen in **Table 4**. Overall, the BET results demonstrate that sulfonation and Zn incorporation significantly modified the surface morphology of the AC catalysts by enhancing surface area, pore volume, and pore structure development. The catalysts predominantly exhibited micro-mesoporous characteristics with increasingly accessible pore networks at higher Zn loadings.

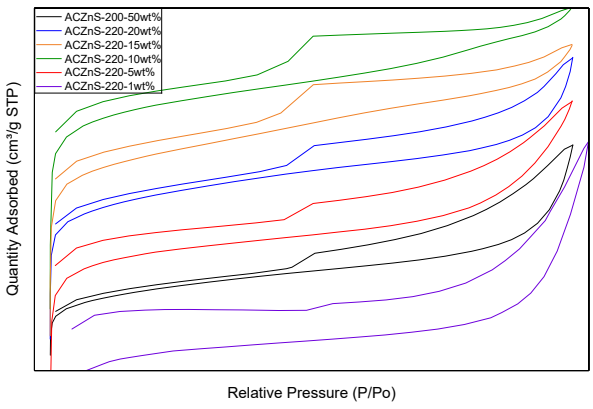
Table 4. Surface morphology and acid properties of catalysts

Catalyst	BET surface area (m2/g)	Pore diameter (nm)	Pore volume (cm3/g)	Micropore volume (cm3/g)	Temperature (°C)	Total acid sites (µmol/g)
ACZn 50	104.11	6.2	0.16	29	-	-
ACZnS 1	8.45	3.3	0.007	6	155	571
					628	4284
ACZnS 5	287.53	2.4	0.18	219	152	480
					615	3374
ACZnS 10	429.64	2.1	0.22	328	251	319
					644	7066
ACZnS 15	410.49	2.3	0.24	280	646	11751
ACZnS 20	482.48	2.7	0.33	293	660	13199
ACZnS 50	600.70	4.2	0.64	214	240	40
					416	22
					646	590
					916	376

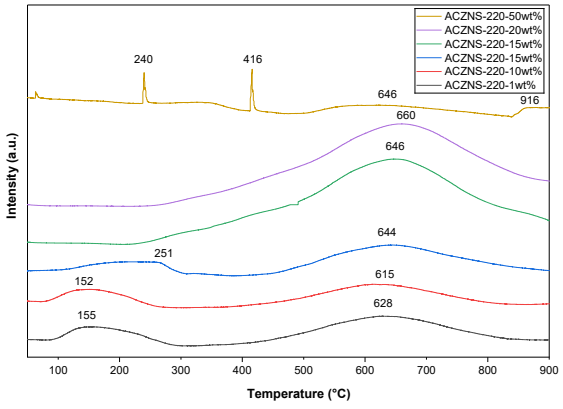
406

407

a



b



408

Figure 3. (a) BET analysis and (b) TPD-NH_3 for ACZnS-220-1wt%, ACZnS-220-5wt%, ACZnS-220-10wt%, ACZnS-220-15wt%, ACZnS-220-20wt% and ACZnS-220-50wt%

The presence of S and Zn may contribute to the change in acidity of the catalyst [14] and the acidity result showed in **Table 4** and **Fig. 3b**. All ACZnS catalysts exhibited dominant NH_3 desorption at high temperatures (>600 °C), indicating that strong acid sites constitute the major acidic species. A smaller low-temperature desorption peak corresponding to weak acid sites (<250 °C) was also observed for several catalysts. The total acidity increased progressively in the order ACZnS-220-50wt% (1030 μmol g^{-1}) < ACZnS-220-5wt% (3855 μmol g^{-1}) < ACZnS-220-1wt% (4855 μmol g^{-1}) < ACZnS-220-10wt% (7446 μmol g^{-1}) < ACZnS-220-15wt% (11752 μmol g^{-1}) < ACZnS-220-20wt% (13199 μmol g^{-1}), demonstrating that increasing ZnS incorporation substantially enhances overall acidity. Notably, ACZn-220-(1–10 wt%) exhibited two NH_3 desorption peaks centered at approximately 152-251 °C and 615-644 °C, corresponding to weak and strong acid sites, respectively [30]. The presence of weak acid sites at low Zn loadings suggests that both native oxygen-containing surface groups and Zn-derived acidic species contribute to the overall acidity. In contrast, catalysts with higher Zn loadings (>10 wt%) were predominantly characterized by strong acid sites, likely due to the increased metal loading and other strongly acidic surface functionalities [30]. Notably, the high Zn-loading catalyst (50 wt.%) was predominantly characterized by strong acid sites; however, it exhibited a marked reduction in total acid density (~1030 μmol g^{-1}). This reduction is attributed to the intrinsic alkaline character of Zn species, which partially neutralizes the acidic sites of the support, thereby decreasing the overall density of accessible acid sites despite the predominance of strong acidity (Kouider Elouahed et al. 2024). Several studies have reported that an efficient esterification catalyst could govern by high acid density with strong acidic sites. Nevertheless, [36] reported that catalytic esterification performance is governed not only by

434 acid strength but also by the accessibility and turnover of active sites. Indeed, excessive strong
435 acid sites can bind reactants and reaction intermediates more strongly, thereby increasing
436 desorption barriers and lowering catalytic turnover. Consequently, catalysts possessing
437 sufficient strong acidity together with a sufficiently high density of accessible acid sites
438 generally exhibit superior esterification performance compared with catalysts having extremely
439 strong acid sites alone. The ACZnS-220-5 wt.% catalyst, which possesses a combination of
440 weak and strong acidic sites with a total acidity of approximately 3854 μmol g^{-1}, was found to
441 be effective for the esterification of FOG. Although the catalyst with a higher Zn loading (10
442 wt.%) exhibited both weak and strong acidic sites and a total acidity approximately 45% greater
443 than that of the 5 wt.% catalyst, this increase in acidity did not translate into enhanced
444 esterification performance. As discussed previously, the additional acid sites did not
445 proportionally increase catalytic activity, suggesting that catalytic performance depends on the
446 accessibility and effective utilization of the acid sites rather than their quantity alone. These
447 findings suggest that esterification is governed by an optimum balance of acid strength and acid
448 site density rather than by an excessive concentration of acidic sites [32]. This interpretation is
449 consistent with the mechanistic review by [12], which emphasizes that esterification
450 performance depends on the combined effects of acid strength, active-site accessibility, pore
451 topology, adsorption, diffusion and hydrophobicity. Therefore, the present study proposes that
452 the ACZnS-220-5 wt.% is attributed to achieving an optimum balance between acid-site density
453 and acid strength while maintaining conditions favourable for effective reactant access to the
454 active sites. Accordingly, ACZnS-220-5 wt.% was selected for further physicochemical
455 characterization.

456 The FESEM images of ACZnS-220-5wt% reveal an irregular and porous carbonaceous
457 morphology with a layered structure. At lower magnifications, the catalyst exhibits elongated
458 sheet-like particles containing numerous pore openings and cavity-like pores with varying sizes

distributed throughout the carbon matrix (**Fig 4a-d**). The morphology consists of both larger cavities and smaller pores embedded within the carbon framework, resulting in a complex porous architecture. These observations indicate that the catalyst possesses a highly textured surface with abundant pore structures and non-uniformly distributed surface features. To further understand the elemental composition and the structure of the catalyst FESEM-EDX for ACZNS-220-5wt% was done. The EDX results confirm that carbon is the dominant element, with an average composition of approximately 73 wt%, which is consistent with the biochar-based carbonaceous support. Oxygen was also detected (~11.6 wt%), indicating the presence of oxygen-containing functional groups such as sulfonic groups introduced during the sulfonation process. Sulfur was present in a relatively high amount (~10.3 wt%), confirming the successful incorporation of sulfonic acid groups, which are responsible for providing strong acidic sites [3]. Approximately, ~4.1 wt% was observed for Zn which is close to the theoretical loading (5 wt%), confirming successful impregnation method. Traces amounts of Si (~0.54 wt%) and Al (~0.08 wt.%) were detected, likely from biomass precursor[23]. Overall, the FESEM–EDX analysis confirms successful Zn sulfonation functionalization and existence of hierarchical pore structure.

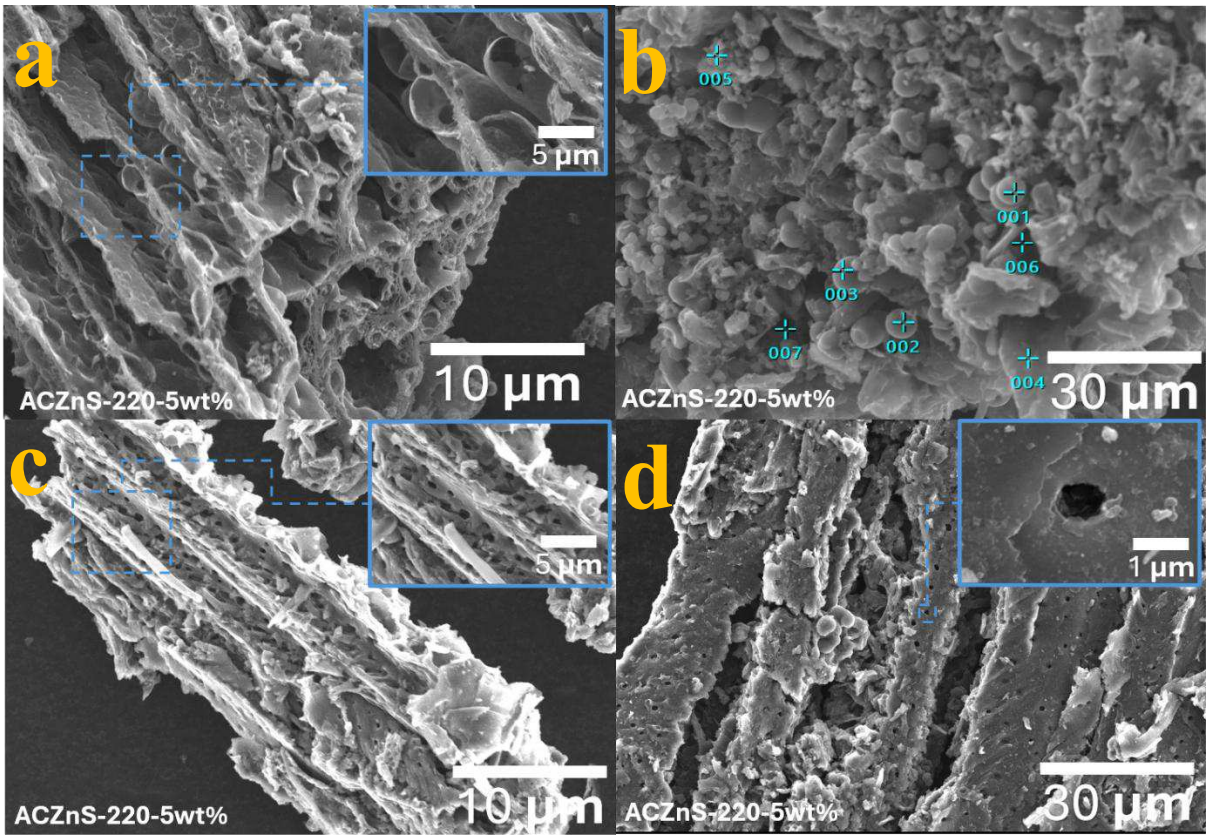


Figure 4. FESEM for ACZnS-220-5wt%

X-ray photoelectron spectroscopy (XPS) was performed to investigate the surface elemental composition of ACZnS-220-5wt% (ACZnS5). The survey spectra revealed the presence of carbon (C), oxygen (O), zinc (Zn) and sulfur (S). Carbon exhibited the highest peak intensity, indicating that the catalyst surfaces remained predominantly carbonaceous after zinc incorporation and sulfonation.The high-resolution C 1s spectra displayed a dominant peak centered at approximately 284 eV (C=C) [21], representing the major carbon contribution on the catalyst surface. The O 1s spectra exhibited broad peaks centered at 531 eV region. The broad peak envelopes suggest the presence C=O species [31]. The relatively high intensity of the O 1s peak suggests the presence of abundant oxygenated groups on the catalyst surface, which may contribute to enhanced surface acidity and catalytic activity. The high-resolution S

2p spectrum can be deconvoluted into two components located at 167.2 eV and 168.5 eV, corresponding to S $2p_{3/2}$ and S $2p_{1/2}$, associated with $–SO_3H$ and C–S respectively [9]. The presence of sulfonic acid functionalities is crucial as they serve as the primary acid sites responsible for catalytic activity. The Zn 2p spectrum displays two characteristic peaks at 1021.8 eV and 1044.7 eV, corresponding to Zn $2p_{3/2}$ and Zn $2p_{1/2}$, respectively. The spin-orbit splitting of approximately 22.9 eV is consistent with Zn^{2+} species, indicating that zinc remains present on the catalyst surface after sulfonation. Overall, the XPS results confirm the successful incorporation of sulfonic acid groups while retaining Zn species and heteroatom functionalities on the catalyst surface[24]. The N 1s spectrum exhibits weak peaks at approximately 398.0 and 400.1 eV. Since nitrogen was not deliberately introduced during catalyst synthesis and the thermal treatment was conducted under an inert nitrogen atmosphere, the detected nitrogen species are likely derived from residual nitrogen-containing compounds inherently present in the precursor material. It is also noted there is no presence of N in edx analysis (**Table 5**). Consequently, the contribution of nitrogen functionalities to the catalytic activity is expected to be minimal to none. The catalytic performance of the material is more likely governed by the presence of sulfonic acid groups, Zn species, and oxygen-containing surface functionalities.

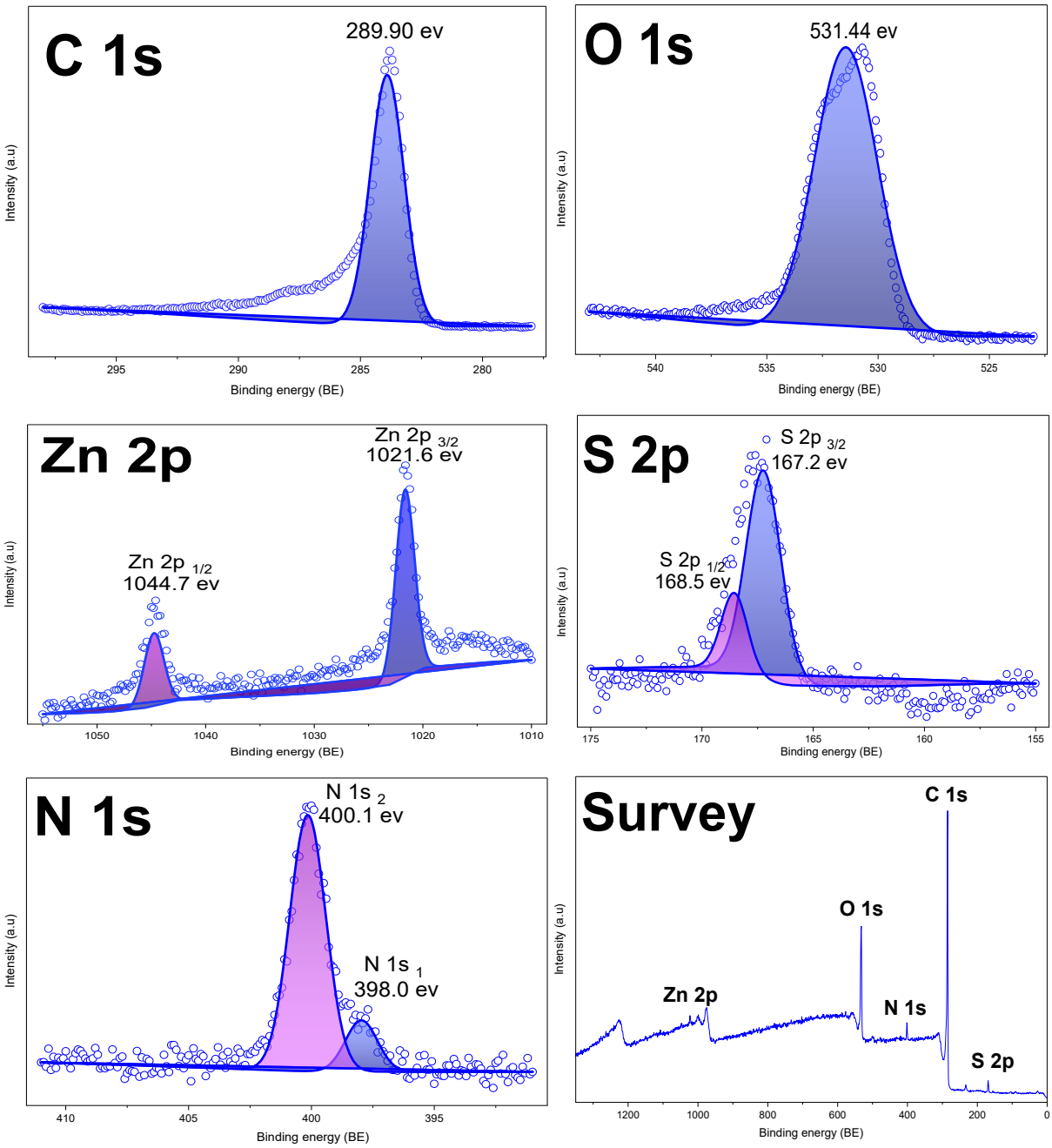


Figure 5. Deconvoluted XPS spectral peak in the C_{1s}, O_{1s}, Zn_{2p}, S_{2p} and N_{1s} structures ACZnS-220-5wt%

FTIR analysis was conducted to verify the surface functional groups present on ACZnS-220-5wt% and to complement the XPS findings. As shown in **Fig. S3**, characteristic absorption bands were observed at and 1036, 1163 1585 1707 and 1982 cm^{-1}. The bands at 1036 cm^{-1} and 1163 cm^{-1} are assigned to stretching vibrations of S=O groups, respectively, confirming the successful incorporation of sulfur-containing functionalities onto the catalyst surface[6][13]. These bands are characteristic of sulfonic acid (-SO_3H) groups commonly reported for

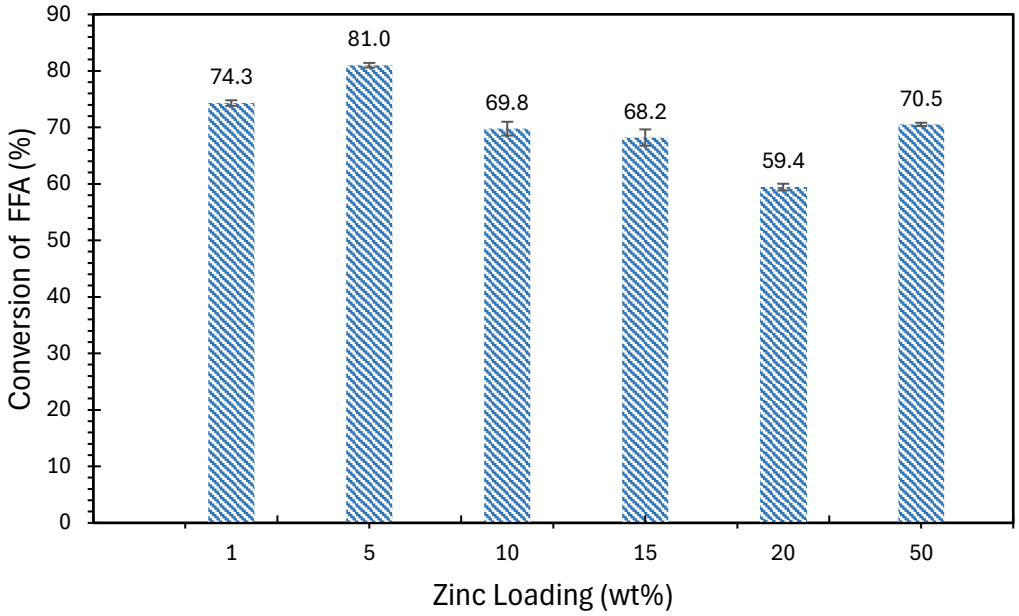
sulfonated carbon catalysts. The presence of sulfur-containing functional groups observed by FTIR is consistent with the S 2p signals detected in the XPS analysis, providing further evidence that sulfonation was successfully achieved. The incorporation of these sulfonic acid groups is expected to contribute significantly to the formation of acid sites, which is in agreement with the high acidity observed in the NH_3-TPD analysis. Furthermore , the bands located at, 1585 cm^{-1} correlates to C=C, [6] while the peak at 1707 cm^{-1} corresponds to aromatic C=O stretching within the carbon framework.

The thermogravimetric analysis (TGA) confirms that the optimized catalyst, **ACZnS-220-5 wt%**, possesses sufficient thermal stability for esterification reactions, which are conducted at temperatures significantly lower than the onset of thermal decomposition. The catalyst exhibited only a minor mass loss below approximately 100 °C (**Fig. S2a**), corresponding to the desorption of physically adsorbed moisture and volatile species [28], while the carbon framework remained stable throughout the reaction temperature range. Furthermore, to elucidate the thermal behavior of the sulfonated catalyst system, the TGA profiles of **ACZn-200-50 wt%** and **ACZnS-200-50 wt%** were compared and the result showed in **Fig. S2b**. Notably, the sulfonated ACZnS catalyst exhibited an additional gradual weight loss between approximately 100 and 450 °C, which is attributed to the thermal decomposition of grafted sulfonic acid (-SO_3H) groups and other oxygen-containing surface functionalities introduced during the sulfonation process [28]. Nevertheless, both catalysts exhibited rapid degradation of the carbonaceous framework between approximately 450 and 550 °C. This weight loss is primarily attributed to the thermal decomposition of the carbon matrix together with the decomposition of thermally labile oxygen-containing surface functional groups, including carboxyl (-COOH), hydroxyl (-OH), carbonyl (C=O), and lactone groups, particularly in catalysts subjected to sulfonation or oxidation. Above 600 °C, the residual mass remained nearly constant up to 1200 °C, indicating the excellent thermal stability of the incorporated Zn-

containing inorganic phases, which did not undergo further decomposition under the applied heating conditions. These findings demonstrate that the acidic functionalities and Zn species incorporated through the synthesis strategy remain thermally stable under the mild esterification (60-100 ^{o}C) conditions.

3.3 Catalytic esterification of FOG

The influence of Zn loading on catalytic activity was investigated to determine the optimal metal content. As 50wt% is not economical, lower Zn loading (1-50 wt.%) was also investigated. The results indicated that increasing Zn loading from 1 wt% to 5 wt% significantly enhanced FFA conversion, suggesting that Zn plays a crucial role in improving catalyst performance. However, further increasing Zn loading beyond 10 wt% resulted in a decrease in catalytic performance. This decline can be attributed primarily to changes in the pore structure and accessibility of the active sites. As shown in **Table 5**, increasing the Zn loading altered the pore diameter and pore volume, which may reduce reactant diffusion and limit access to the active acid sites despite the higher total acidity. Consequently, the 5 wt.% Zn-loaded catalyst provides an optimal balance between acid-site density with optimal turn over active sites and pore accessibility, resulting in superior esterification performance. Therefore, the superior activity of ACZnS-220-5 wt.% is attributed mainly to its favourable pore characteristics and accessible acid sites.



559

560 **Figure 6.** FFA conversion of different weight percentage of zinc loading [1wt%, 5wt%,

561 10wt%, 15wt%, 20wt%, and 50wt%]

562

563 *3.3 Optimization of parametric studies*

564 The optimization of reaction parameters was subsequently performed using the One

565 Variable-At-a-Time (OVAT) approach to determine the optimal operating conditions for FOG

566 esterification. The effect of reaction temperature was first examined, revealing that FFA

567 conversion increased with temperature 70 °C. Higher temperatures increase reaction rates by

568 providing sufficient energy to overcome activation barriers. Additionally, higher temperatures

569 reduce the viscosity of FOG, improving mass transfer and enhancing contact between reactants

570 and catalyst [19]. However, further increases in temperature beyond 80 °C did not result in

571 significant improvement and reduces conversion. This is primarily due to the evaporation of

572 methanol at elevated temperatures, which decreases its concentration in the reaction mixture

and limits the forward reaction. Moreover, excessive temperatures may promote side reactions or lead to thermal degradation of reactants [3].

The methanol-to-oil ratio also plays a critical role in determining the equilibrium position of the esterification reaction. Increasing the ratio from 10:1 to 25:1 resulted in a significant increase in FFA conversion, as excess methanol shifts the equilibrium toward ester formation. However, further increases beyond 20:1 did not yield substantial improvements and remained stagnant. Excessive methanol does not react with the oil as optimum level of methanol is achieved [28]. Additionally, higher methanol usage increases separation and recovery costs, making the process less economically favorable.

The effect of reaction time showed that FFA conversion increased rapidly during the initial stages of the reaction and reached equilibrium at approximately 2 h. This behavior indicates that the reaction is kinetically controlled at early stages and gradually transitions to equilibrium control. Short reaction times result in incomplete conversion due to insufficient contact between reactants and catalysts, while excessively long reaction times do not significantly improve conversion and may cause back reaction [37]. In some cases, prolonged reaction times may also lead to reverse reactions, reducing overall efficiency[9].

Catalyst loading was found to have a significant impact on the esterification process. Increasing catalyst loading up to 3 wt.% resulted in higher FFA conversion due to the increased availability of active sites. However, further increases beyond this value led to a decrease in conversion, which can be attributed to mass transfer limitations and increased viscosity of the reaction mixture [19]. High catalyst loading may also lead to particle aggregation, reducing the effective surface area and limiting the accessibility of active sites [16]. Therefore, 3 wt% catalyst loading was identified as the optimal condition. Under the optimized conditions of 3 wt% catalyst loading, 20:1 methanol-to-oil ratio, 70 °C reaction temperature, and 2 h reaction

time, the ACZnS-220-5wt% catalyst achieved a FAME yield of approximately 81%. This represents a significant improvement compared to the preliminary conversion, highlighting the importance of systematic optimization. The high conversion achieved under relatively mild conditions demonstrates the efficiency of the developed catalyst system.

Table 6. Transesterification reaction responses based OVAT design.

No.		Factor variables				Conversion rate of FFA (%)
Run	Optimization type	A: Temperature (°C)	B: Methanol to oil ratio	C : Time (h)	D: Catalyst concentration (wt%)	
1	Temp	60	1 :14	2	3	73.5
2	Temp	70	1 :14	2	3	81.0
3	Temp	80	1 :14	2	3	78.1
4	Temp	100	1 :14	2	3	77.3
5	Ratio	70	1 :10	2	3	65.0
6	Ratio	70	1 :14	2	3	81.0
7	Ratio	70	1 :20	2	3	81.8
8	Ratio	70	1 :25	2	3	81.6
9	Time	70	1 :20	1	3	42.2
10	Time	70	1 :20	2	3	81.8
11	Time	70	1 :20	3	3	70.2
12	Time	70	1 :20	5	3	80.5
13	Cat%	70	1 :20	2	1	6.3
14	Cat%	70	1 :20	2	3	81.8

15	Cat%	70	1 :20	2	5	70.0
16	Cat%	70	1 :20	2	7	69.4

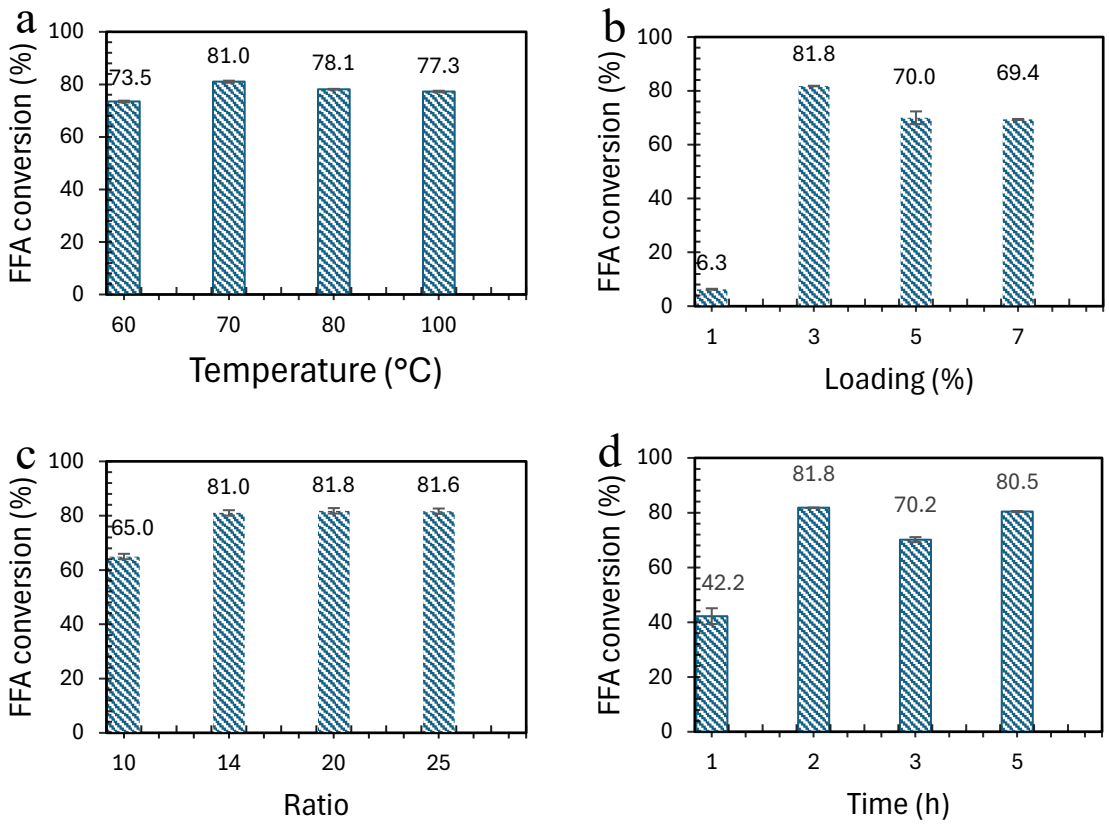


Figure 7. FFA conversion of different optimization conditions (a) Reaction temperature against FFA conversion [Fixed : 1 :14 methanol-to oil molar ratio, 3wt% catalyst loading and 2h reaction time Changed : 60 °C, 70 °C 80 °C and 100 °C] (b) Catalyst loading against FFA conversion [Fixed : 70 °C reaction temperature, 1 :20 methanol-to oil molar ratio and 2h reaction time Changed : 1wt%, 3wt%, 5wt% and 7wt%], (c) Methanol-to oil molar ratio against FFA conversion [Fixed : 70 °C reaction temperature, 3wt% catalyst loading and 2h reaction time Changed : 1 :10, 1 :14, 1 :20 and 1 :25] and (d) Reaction time against FFA conversion [Fixed : 70 °C reaction temperature, 3wt% catalyst loading and 1 :20 methanol-to oil molar ratio Changed : 1h, 2h, 3h and 5h].

GC-MS analysis was employed to qualitatively evaluate the compositional changes of the feedstock before and after esterification. As illustrated in **Fig. 8**. the raw FOG sample was dominated by FFA, which constituted 94.64% of the detected compounds. The major FFAs identified were n-hexadecanoic acid (52.37%) and oleic acid (38.21%). Following esterification, the biodiesel product exhibited a substantial reduction in acid-type compounds to 0.90%, while ester-type compounds (methyl palmitate and methyl oleate, along with minor amounts of methyl linoleate, methyl stearate, and methyl myristate) (biodiesel) (based on NIST library matching >98%) increased markedly to 92.94%. The reduction of the major FFAs provides strong qualitative evidence of successful conversion. Specifically, palmitic acid decreased from 52.37% to 0.36%, corresponding to a 99.31% reduction. Similarly, oleic acid decreased from 38.21% to 0.35%, corresponding to a 99.08% reduction. Noted, the total FFA species in the FOG detected by GCMS also decreased from 94.64% to 0.90% in the biodiesel product, indicate that the major FFA present in the FOG were effectively transformed into methyl ester-type compounds during the esterification reaction [16]. Indeed, the GC–MS results are consistent with the GC–FID findings, showing that the predominant ester species detected were methyl palmitate (C16:0) and methyl oleate (C18:1) (**Fig. 8**) with FAME yield ~90%. These results confirm the effectiveness of the ACZnS-220-5wt% catalyst in promoting the conversion of FFA into FAME.

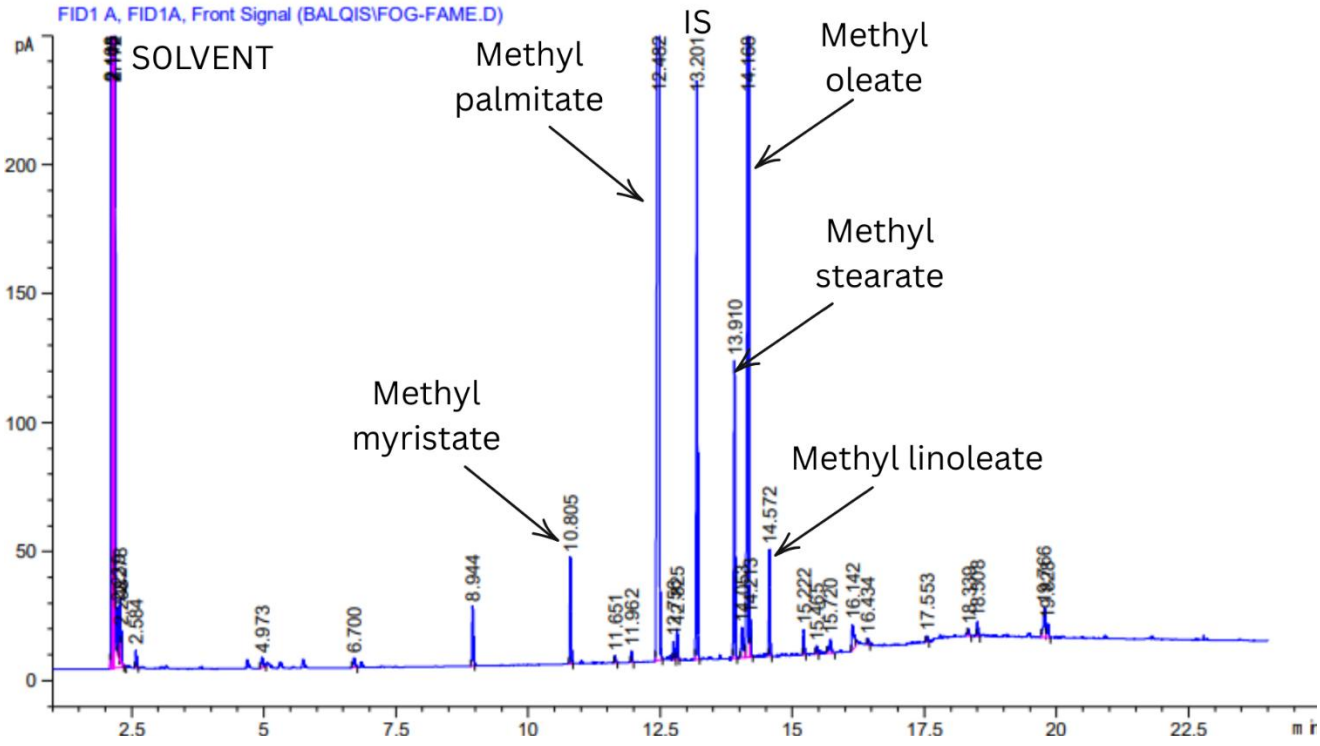


Figure 8. GC-FID analysis of optimized biodiesel

Table 7. Summary of GC-MS results of raw FOG and optimized biodiesel

Fuel content	FFA mass (wt%)	FAME mass (wt%)
Acid	94.64	0.90
Methyl ester	0.69	92.94
Others *	4.67	6.16

*1-Decanol, 2-hexyl-,2(3H)-Furanone, dihydro-5-pentyl-,Di-n-octyl phthalate and Nonanal

3.4 Proposed mechanism of esterification

A plausible mechanism for the esterification of FOG over the ACZnS-220-5 catalyst is proposed in **Fig. 9.** The catalytic activity is mainly attributed to the acid sites (–SO_3H) anchored on the sulfonated carbon surface. These acidic groups donate protons to the reaction medium and activate the carboxylic acid functionalities present in the FOG feedstock. Initially, protonation of the carbonyl oxygen increases the electrophilic character of the carbonyl carbon, facilitating nucleophilic attack by methanol. This interaction forms a tetrahedral intermediate, which subsequently undergoes proton transfer and elimination of a water molecule. The

reaction ultimately produces methyl ester compounds, while the active –SO_3H site on the ACZnS catalyst is regenerated and remains available for subsequent catalytic cycles. The incorporated Zn species are proposed to stabilize the sulfonic acid groups on the carbon framework through Zn–S interactions, thereby contributing to catalyst structural stability and good reusability over repeated reaction cycles. The proposed overall mechanism demonstrates that ACZnS facilitates the conversion of acidic components in FOG into methyl ester products through acid-catalyzed esterification, without attributing the pathway to any specific individual FFA species.

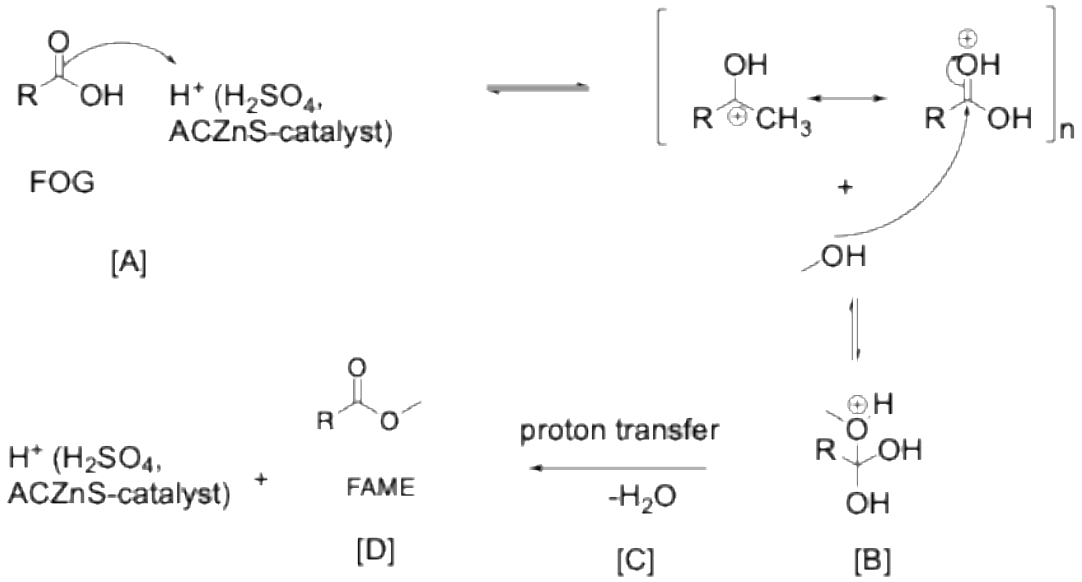


Figure 9. Proposed mechanism pathways for esterification of FOG

3.5 Reusability

The reusability trend observed in this study shows that the catalyst exhibits high catalytic activity during the initial cycle, followed by a gradual decline in performance with repeated use. In the first cycle, the catalyst achieves high FFA conversion and biodiesel yield, indicating that the active sites are fully available and functioning effectively. However, from the second cycle onward, a noticeable decrease in conversion is observed, and this decline continues progressively up to the fifth cycle. Although the catalyst does not completely lose its activity, the reduction in performance confirms that some level of deactivation occurs during

repeated reactions **Fig10**. This behavior is primarily attributed to the stability of the sulfonic acid (–SO_3H) functional groups, which serve as the main active sites for the esterification reaction. The incorporation of zinc plays an important role in enhancing catalyst stability through the formation of strong Zn–S interactions. These interactions help anchor the sulfonic groups more firmly onto the carbon surface, thereby reducing the rate of sulfur leaching compared to conventional sulfonated carbon catalysts. As a result, the catalyst demonstrates improved reusability, particularly in the early cycles where the active sites remain largely intact. Despite the improved stability imparted by zinc but is not sufficiently strong to completely prevent the loss of active sites during repeated reaction cycles. This is supported by the NH_3-TPD analysis, where the total acidity decreased from 3885.29 to 3187.90 μmol g^{-1} after reuse, corresponding to an approximately 18% reduction in the total number of acid sites. The decrease is primarily associated with the strong acid sites, which dropped from 3374.36 to 2217.31 μmol g^{-1}, while the proportion of weak acid sites increased from 12.47% to 30.45%, indicating that a significant fraction of the strong acid sites responsible for esterification was lost or transformed into weaker acidic sites.

The FTIR spectra of the fresh and spent catalysts exhibit absorption bands at approximately 1703, 1584, 1163, and 1034 cm^{-1} for the fresh catalyst and 2914, 2850, 1731, 1573, 1462, 1152, and 1030 cm^{-1} for the spent catalyst, indicating that the principal functional groups are retained after catalyst reuse. The additional absorption bands observed at 2914 and 2850 cm^{-1} in the spent catalyst are assigned to the asymmetric and symmetric stretching vibrations of aliphatic –CH_2/–CH_3 groups, while the band at 1462 cm^{-1} corresponds to CH_2 bending (scissoring) vibrations. The appearance of these bands after repeated use may be attributed to the adsorption of residual FFAs, methyl esters, glycerol, or other organic intermediates/products from the esterification reaction on the catalyst surface, suggesting incomplete removal during the regeneration process [37]. The accumulation of these organic

687 species can partially cover the catalyst surface and block pores, thereby hindering the diffusion
688 of reactants to the active acid sites and reducing the number of accessible catalytic sites. Such
689 surface fouling is a common cause of catalyst deactivation during repeated esterification cycles
690 and is consistent with the decrease in acidity observed by NH_3-TPD analysis (see **Table S3,**
691 **Figure S6**). The persistence of the sulfate-related bands at 1163/1034 cm^{-1} (fresh) and
692 1152/1030 cm^{-1} (spent) indicates that sulfate species remain anchored to the catalyst surface
693 after reuse, although slight shifts in the band positions may reflect changes in the local chemical
694 environment of the sulfate groups due to catalyst use or interactions with adsorbed species [13].
695 Surface restructuring during repeated esterification and regeneration may have enhanced the
696 accessibility of oxygen-containing and sulfur-containing functionalities to infrared radiation.
697 Overall, the reusability trend indicates that the catalyst possesses moderate stability and can be
698 reused multiple times, but with a gradual loss in efficiency which is better than Fadillah et al's
699 finding [16], where only regeneration through repeated sulfonation was able to increase the
700 reusability of catalyst and immediate drop-in activity if only methanol washing is done. Thus,
701 suggested that addition of Zn is effective in maintaining catalyst stability with only methanol
702 washing. The presence of zinc enhances the durability of the catalyst compared to non-metal-
703 doped systems; however, further improvements are necessary to achieve long-term stability and
704 consistent performance. This suggests that future work should focus on strengthening the
705 interaction between active sites and the catalyst support to further minimize leaching and extend
706 catalyst lifespan.

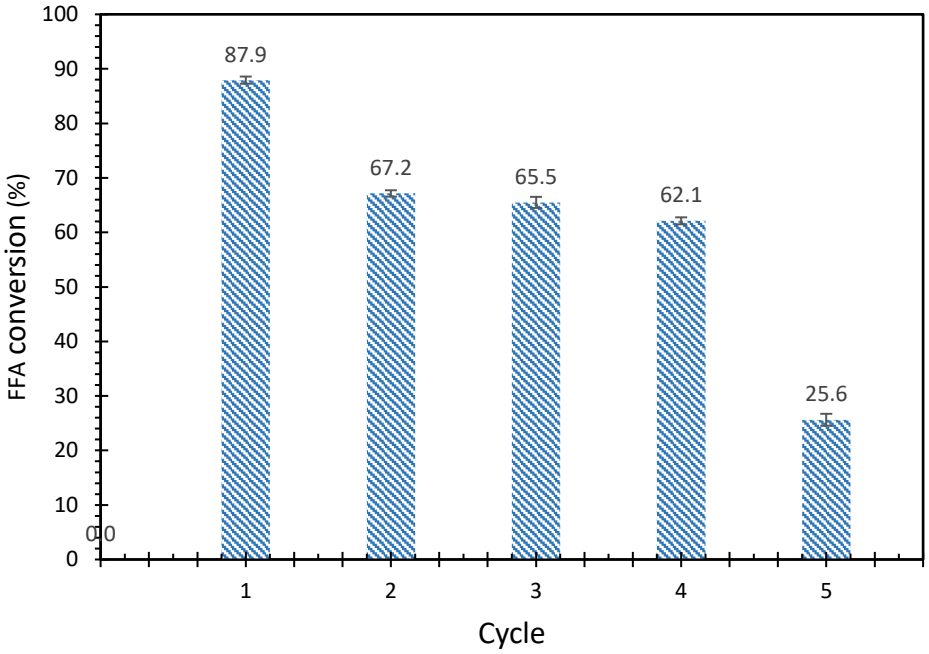


Figure 10. Reusability of catalyst after methanol washing under the optimum reaction conditions of 70 °C, a 20:1 methanol-to-oil ratio, 3 wt.% catalyst loading, and 2 h reaction time

4. Conclusion

The present study successfully developed series of Zn (1-50 wt.%)-sulfonated activated carbon catalyst derived from sunflower seed husk for the esterification of high-FFA FOG into biodiesel. Hydrothermal carbonization demonstrated that increasing the treatment temperature enhanced carbonization and aromatization of the sunflower husk, with 220 °C providing a suitable balance between carbon enrichment and structural preservation. XRD confirmed the formation of Zn-containing crystalline phases and the preservation of the carbon framework, while subsequent sulfonation altered the Zn-containing phases and promoted a more dispersed structure. FTIR and XPS further confirmed the successful incorporation of sulfur-containing and sulfonic acid functionalities together with Zn species on the carbon surface. Among the synthesized catalysts, ACZnS-220-5wt% exhibited the highest catalytic performance, with a BET surface area of 287.53 $m^2\ g^{-1}$ and total acidity of 3855 $\mu mol\ g^{-1}$, providing an optimal

balance of acid-site density, acid strength, and pore accessibility. Although higher Zn loadings increased surface area and acidity, they did not improve catalytic performance, demonstrating that accessible active sites are more important than maximum surface area or acidity alone. Under the optimum reaction conditions of 70 °C, a 20:1 methanol-to-oil ratio, 3 wt.% catalyst loading, and 2 h reaction time, the catalyst achieved 88% FFA conversion while GC–MS and GC–FID analyses confirmed 98 % efficient conversion of FFAs into FAMEs. Reusability studies further demonstrated that Zn incorporation improved catalyst stability by reducing sulfur leaching relative to conventional sulfonated carbon catalysts, although gradual deactivation still occurred because of the loss of strong acid sites and surface fouling during repeated use. Overall, this work demonstrates that Zn-assisted stabilization of sulfonated biomass-derived carbon is an effective strategy for producing reusable heterogeneous acid catalysts for sustainable biodiesel production from waste FOG, while providing a promising platform for future studies on biomass-derived solid acid catalysts, including the incorporation of alternative metal promoters and the optimization of catalyst architecture to further enhance catalytic performance, stability, and industrial applicability for renewable biodiesel production for harsh feed as FOG.

References

[1] Abd El Fatah Abomohra, Mahdy Elsayed, Sivakumar Esakkimuthu, Mostafa El-Sheekh, and Dieter Hanelt. 2020. Potential of fat, oil and grease (FOG) for biodiesel production: A critical review on the recent progress and future perspectives. *Progress in Energy and Combustion Science 81*. https://doi.org/10.1016/j.pecs.2020.100868

[2] N. Ahmed, A. Straub, and M. Ali. 2026. Fats, oil, and grease (FOG) in wastewater: sources, mechanisms, control, and removal strategies. *International Journal of Environmental Science and Technology 23*. https://doi.org/10.1007/s13762-025-06977-2

[3] Rawaz Ahmed and Katherine Huddersman. 2022. Review of biodiesel production by the esterification of wastewater containing fats oils and grease (FOGs). *Journal of Industrial and Engineering Chemistry 110*, 1–14. https://doi.org/10.1016/j.jiec.2022.02.045

[4] Muntathir Albeladi, Mohammed H. Geesi, Yassine Riadi, Mustapha Alahiane, Talal A. Aljohani, Avni Berisha, Arianit Reka, Abdellah Kaiba, and Oussama Ouerghi. 2023. Synergistic inhibitive effect of a hybrid zinc oxide-benzalkonium chloride composite on the corrosion of carbon steel in a sulfuric acidic solution. *Green Processing and Synthesis* 12, 1 (January 2023). https://doi.org/10.1515/gps-2023-0139

[5] Ali Al-Saadi, Bobby Mathan, and Yinghe He. 2020. Biodiesel production via simultaneous transesterification and esterification reactions over SrO–ZnO/Al2O3 as a bifunctional catalyst using high acidic waste cooking oil. *Chemical Engineering Research and Design* 162, (October 2020), 238–248. https://doi.org/10.1016/j.cherd.2020.08.018

[6] Morteza Asemani and Ahmad Reza Rabbani. 2020. Detailed FTIR spectroscopy characterization of crude oil extracted asphaltenes: Curve resolve of overlapping bands. *J. Pet. Sci. Eng.* 185, (February 2020). https://doi.org/10.1016/j.petrol.2019.106618

[7] Progna Banerjee and Prashant K. Jain. 2018. Mechanism of sulfidation of small zinc oxide nanoparticles. *RSC Adv.* 8, 60 (2018), 34476–34482. https://doi.org/10.1039/c8ra06949b

[8] Jack Clohessy and Witold Kwapinski. 2020. Carbon-based catalysts for biodiesel production-A review. *Applied Sciences (Switzerland) 10*. https://doi.org/10.3390/app10030918

[9] Michelle P. Duarte, Luis Páramo, and Rafik Naccache. 2025. Microwave-assisted synthesis of a sulfonated carbon-based catalyst for efficient esterification of oleic acid into biodiesel. *Catal. Sci. Technol.* (2025). https://doi.org/10.1039/d5cy00736d

[10] Pin Gao, Yiyuan Zhou, Fang Meng, Yihui Zhang, Zhenhong Liu, Wenqi Zhang, and Gang Xue. 2016. Preparation and characterization of hydrochar from waste eucalyptus bark by hydrothermal carbonization. *Energy* 97, (February 2016), 238–245. https://doi.org/10.1016/j.energy.2015.12.123

[11] Lihan Ge, Mahmoud M. Ali, Ahmed I. Osman, Ahmed M. Elgarahy, M. Samer, Yongdong Xu, and Zhidan Liu. 2025. A critical review on conversion technology for

liquid biofuel production from lignocellulosic biomass. *Renewable and Sustainable Energy Reviews 217*. https://doi.org/10.1016/j.rser.2025.115726

[12] Glaucio José Gomes, María Fernanda Zalazar, Janine Carvalho Padilha, Michelle Budke Costa, Claudio Leones Bazzi, and Pedro Augusto Arroyo. 2024. Unveiling the mechanisms of carboxylic acid esterification on acid zeolites for biomass-to-energy: A review of the catalytic process through experimental and computational studies. *Chemosphere 349*. https://doi.org/10.1016/j.chemosphere.2023.140879

[13] Qingqing Guan, Yi Li, Yuan Chen, Yuzhen Shi, Junjie Gu, Bin Li, Rongrong Miao, Qiuling Chen, and Ping Ning. 2017. Sulfonated multi-walled carbon nanotubes for biodiesel production through triglycerides transesterification. *RSC Adv.* 7, 12 (2017), 7250–7258. https://doi.org/10.1039/c6ra28067f

[14] Lili Huang, Caicheng Song, Yingcen Liu, Hua Lin, Wanyue Ye, He Huang, Rongwen Lu, and Shufen Zhang. 2021. Enhancement of catalytic esterification by tuning molecular diffusion in sulfonated carbon. *Microporous and Mesoporous Materials* 318, (April 2021). https://doi.org/10.1016/j.micromeso.2021.111024

[15] Husain Husain, Irwan Ramli, Wisnu Ari Adi, Yunasfi Yunasfi, Mashadi Mashadi, Ade Mulyawan, Didin Sahidin Winatapura, Subaer Subaer, Yana Taryana, Yuyu Wahyu, Nurmala Dewi, and Agus Susanto. 2025. Sustainable Synthesis and Structural Characterization of Carbon, Graphite, Graphene Oxide, and Reduced Graphene Oxide Derived from Coconut Shells. *Indonesian Journal of Chemistry* 25, 6 (December 2025), 1768–1777. https://doi.org/10.22146/ijc.105467

[16] S. Fadhilah Ibrahim, N. Asikin-Mijan, M. Lokman Ibrahim, G. Abdulkareem-Alsultan, Saiman Mohd Izham, and Y. H. Taufiq-Yap. 2020. Sulfonated functionalization of carbon derived corncob residue via hydrothermal synthesis route for esterification of palm fatty acid distillate. *Energy Convers. Manag.* 210, (April 2020). https://doi.org/10.1016/j.enconman.2020.112698

[17] Melanie Iwanow, Tobias Gärtner, Volker Sieber, and Burkhard König. 2020. Activated carbon as catalyst support: Precursors, preparation, modification and characterization. *Beilstein Journal of Organic Chemistry 16*, 1188–1202. https://doi.org/10.3762/bjoc.16.104

[18] Yosuke Kikuchi, Qingrong Qian, Motoi Machida, and Hideki Tatsumoto. 2006. Effect of ZnO loading to activated carbon on Pb(II) adsorption from aqueous solution. *Carbon N. Y.* 44, 2 (February 2006), 195–202. https://doi.org/10.1016/j.carbon.2005.07.040

[19] Salima Kouider Elouahed, N. Asikin-Mijan, Abdulkareem Alsultan G., Omar Kaddour, M. R. Yusop, Hadj Mimoun, Salma Samidin, Nasar Mansir, and Y. H. Taufiq-Yap. 2024. Optimization of the activity of Mo7-Zn3/CaO catalyst in the transesterification of waste cooking oil into sustainable biodiesel via response surface methodology. *Energy Convers. Manag.* 303, (March 2024). https://doi.org/10.1016/j.enconman.2024.118185

[20] Baihong Li, Chao Li, Dianqiang Li, Lijun Zhang, Shu Zhang, Zhenhua Cui, Dong Wang, Yonggui Tang, and Xun Hu. 2023. Activation of pine needles with zinc chloride: Evolution of functionalities and structures of activated carbon versus increasing temperature. *Fuel Processing Technology* 252, (December 2023). https://doi.org/10.1016/j.fuproc.2023.107987

[21] Zhijun Li, Shuangling Jin, Rui Zhang, Xia Shao, Shimin Zhang, Ning Jiang, Minglin Jin, Tingting Meng, and Yanhan Mu. 2016. Adsorption of thiophene, dibenzothiophene, and 4,6-dimethyl dibenzothiophene on activated carbons. *Adsorption Science and Technology* 34, 2–3 (March 2016), 227–243. https://doi.org/10.1177/0263617415623439

[22] Rui Ma, Clément Levard, F. Marc Michel, Gordon E. Brown, and Gregory V. Lowry. 2013. Sulfidation mechanism for zinc oxide nanoparticles and the effect of sulfidation on their solubility. *Environ. Sci. Technol.* 47, 6 (March 2013), 2527–2534. https://doi.org/10.1021/es3035347

[23] Irena Matyasik, Joanna Brzeszcz, Małgorzata Labus, Małgorzata Kania, Maja Mroczkowska-Szerszeń, and Lidia Dudek. 2025. The effect of microbiological pretreatment on pyrolysis process of sunflower husk. *J. Environ. Manage.* 379, (April 2025). https://doi.org/10.1016/j.jenvman.2025.124861

[24] Neli Mintcheva, Gospodinka Gicheva, Marinela Panayotova, and Sergei A. Kulinich. 2020. Room-temperature synthesis of zns nanoparticles using zinc xanthates as molecular precursors. *Materials* 13, 1 (January 2020). https://doi.org/10.3390/ma13010171

[25] P. Muthirulan, M. Meenakshisundararam, and N. Kannan. 2013. Beneficial role of ZnO photocatalyst supported with porous activated carbon for the mineralization of alizarin cyanin green dye in aqueous solution. *J. Adv. Res.* 4, 6 (November 2013), 479–484. https://doi.org/10.1016/j.jare.2012.08.005

[26] Usman Idris Nda-Umar, Irmawati Ramli, Ernee Noryana Muhamad, Norsahida Azri, and Yun Hin Taufiq-Yap. 2020. Optimization and Characterization of Mesoporous Sulfonated Carbon Catalyst and Its Application in Modeling and Optimization of Acetin Production. *Molecules* 25, 22 (November 2020). https://doi.org/10.3390/MOLECULES25225221

[27] Thanh Binh Nguyen, Thi Kim Tuyen Nguyen, Wei Hsin Chen, Chiu Wen Chen, Xuan Thanh Bui, Anil Kumar Patel, and Cheng Di Dong. 2023. Hydrothermal and pyrolytic conversion of sunflower seed husk into novel porous biochar for efficient adsorption of tetracycline. *Bioresour. Technol.* 373, (April 2023). https://doi.org/10.1016/j.biortech.2023.128711

[28] Samuel Lalthazuala Rokhum, Bishwajit Changmai, Thomas Kress, and Andrew E.H. Wheatley. 2022. A one-pot route to tunable sugar-derived sulfonated carbon catalysts for sustainable production of biodiesel by fatty acid esterification. *Renew. Energy* 184, (January 2022), 908–919. https://doi.org/10.1016/j.renene.2021.12.001

[29] Dhishna Fanish Rutah, Ackmez Mudhoo, and Dinesh Surroop. 2026. Effects of process parameters on transesterification of waste cooking oil for biodiesel production: a review. *Chemical Papers*. https://doi.org/10.1007/s11696-026-04742-4

[30] Serly Jolanda Sekewael, Remi Ayu Pratika, Latifah Hauli, Amalia Kurnia Amin, Maisari Utami, and Karna Wijaya. 2022. Recent Progress on Sulfated Nanozirconia as a Solid Acid Catalyst in the Hydrocracking Reaction. *Catalysts 12*. https://doi.org/10.3390/catal12020191

[31] Phiraphon Setsuwan, Pareenat Waenthongkham, Kanyaphat Torboon, Yuvarat Ngernyen, Supinya Nijpanich, Andrew J. Hunt, Oue-artorn Limtragool, and Pakin Noppawan. 2026. Efficient and green Biginelli reactions in palm oil using a ZnCl2-impregnated sulfonated carbon catalyst derived from corn cob waste. *Sci. Rep.* (January 2026). https://doi.org/10.1038/s41598-025-34164-3

[32] Juanli Shi, Lina Zhang, and Zhenmin Cheng. 2021. Design of Water-Tolerant Solid Acids: A Trade-Off Between Hydrophobicity and Acid Strength and their Catalytic Performance in Esterification. *Catalysis Surveys from Asia 25*, 279–300. https://doi.org/10.1007/s10563-021-09334-8

[33] Shobhana-Gnanaserkhar, N. Asikin-Mijan, G. AbdulKareem-Alsultan, Sivasangar-Seenivasagam, Saiman Mohd Izham, and Y. H. Taufiq-Yap. 2020. Biodiesel production via simultaneous esterification and transesterification of chicken fat oil by mesoporous sulfated Ce supported activated carbon. *Biomass Bioenergy* 141, (October 2020). https://doi.org/10.1016/j.biombioe.2020.105714

[34] Soroush Soltani, Umer Rashid, Saud Ibrahim Al-Resayes, and Imededdine Arbi Nehdi. 2017. Sulfonated mesoporous ZnO catalyst for methyl esters production. *J. Clean. Prod.* 144, (February 2017), 482–491. https://doi.org/10.1016/j.jclepro.2016.12.128

[35] A. Suemanotham, L. Attanatho, N. Prasongthum, W. Sisuthog, T. Laosombut, and Y. Thanmongkhon. 2022. Upgrading of palm empty fruit bunch for solid biofuel production through hydrothermal carbonization. In *Journal of Physics: Conference Series*, February 04, 2022. IOP Publishing Ltd. https://doi.org/10.1088/1742-6596/2175/1/012031

[36] Kaewta Suwannakarn, Edgar Lotero, and James G. Goodwin. 2007. Solid brønsted acid catalysis in the gas-phase esterification of acetic acid. *Ind. Eng. Chem. Res.* 46, 22 (October 2007), 7050–7056. https://doi.org/10.1021/ie070536u

[37] Xinlong Tie, Yun Li, Kai Yuan, Zhengxin Tan, Yitian Zhang, Jiang Liu, Hongyan Wang, Chengjia Zhang, Yuanzhe Wan, Chong Zou, Tielin Wang, Weiliang Feng, and Xiaoling Duan. 2025. Functionalized chitosan-derived porous carbon as a promising catalyst in one-pot conversion of soybean oil to biodiesel. *Renew. Energy* 245, (June 2025). https://doi.org/10.1016/j.renene.2025.122871

[38] Yuting Wang, Guanyi Chen, Lei Li, and Xiaoqiang Cui. 2022. Stability and carbon sequestration potential of hydrochar derived from Cyperus alternifolius. *Journal of Agro-Environment Science* 41, 3 (2022), 639–647. https://doi.org/10.11654/jaes.2021-0728

[39] Katarzyna Wystalska, Anna Kwarciak-Kozłowska, and Renata Włodarczyk. 2023. Influence of Technical Parameters of the Pyrolysis Process on the Surface Area, Porosity, and Hydrophobicity of Biochar from Sunflower Husk Pellet. *Sustainability (Switzerland)* 15, 1 (January 2023). https://doi.org/10.3390/su15010394

[40] Nidhi Yadav, Gaurav Yadav, and Md Ahmaruzzaman. 2023. Biomass-derived sulfonated polycyclic aromatic carbon catalysts for biodiesel production by esterification reaction. *Biofuels, Bioproducts and Biorefining* 17, 5 (2023), 1343–1367. https://doi.org/10.1002/bbb.2486

[41] Bing Yan, Jiaojiao Zheng, Feng Wang, Luying Zhao, Qian Zhang, Wenhui Xu, and Shuijian He. 2021. Review on porous carbon materials engineered by ZnO templates: Design, synthesis and capacitance performance. *Materials and Design 201*. https://doi.org/10.1016/j.matdes.2021.109518

910

Supplementary data

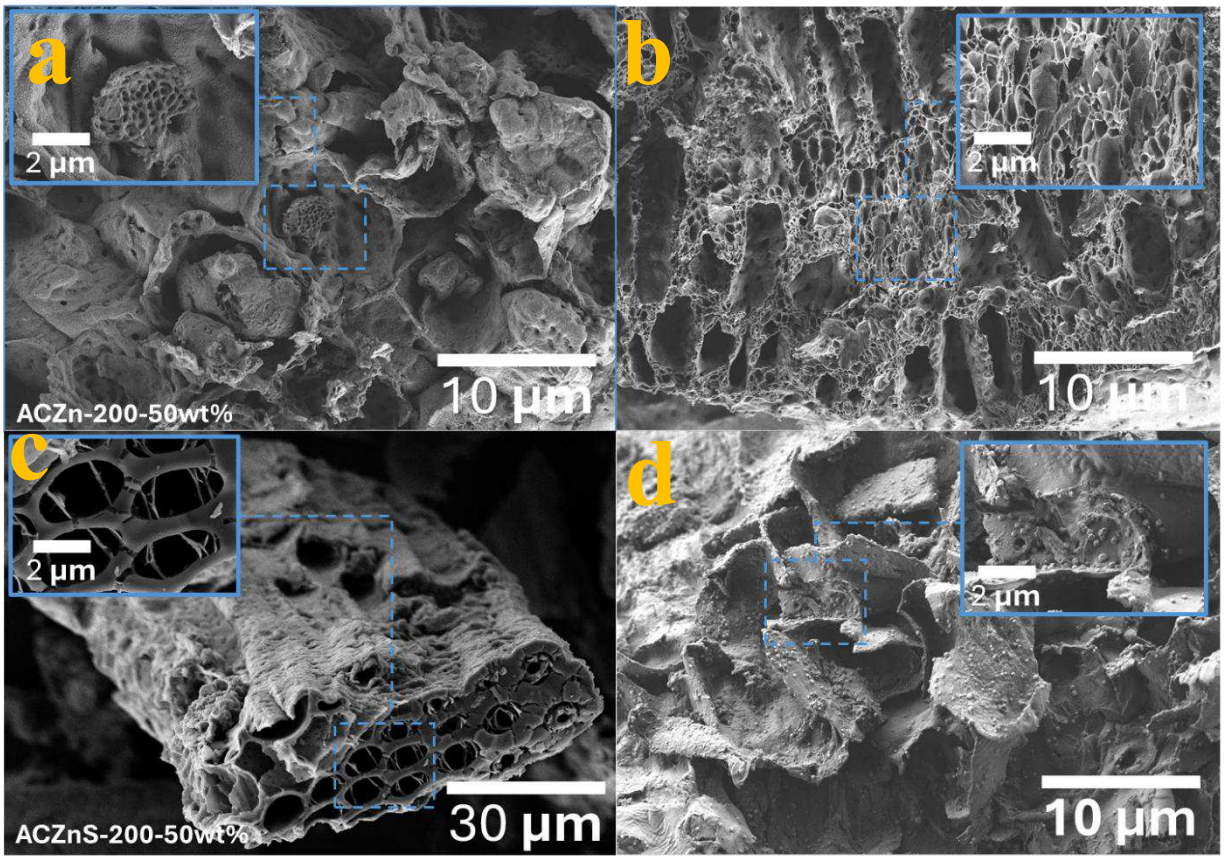


Figure S1. FESEM images for ACZn-200-50wt% and ACZnS-200-50wt%

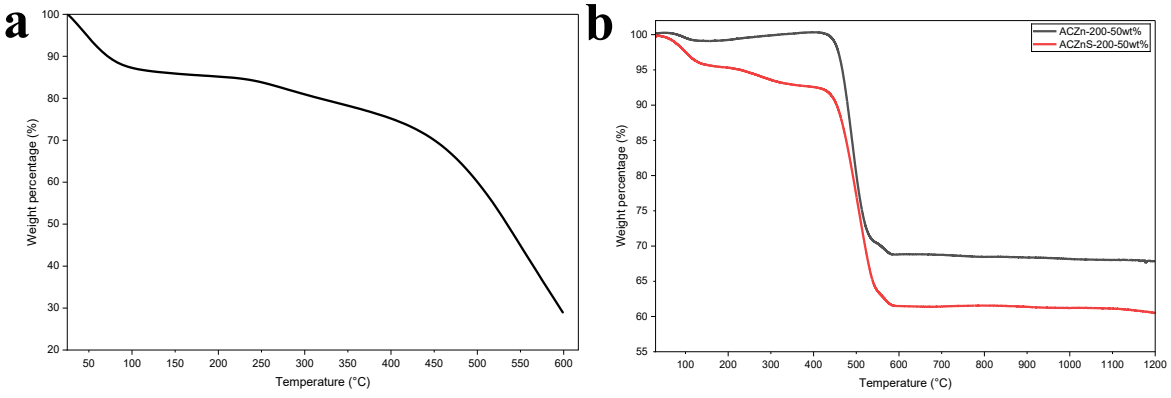


Figure S2. TGA analysis (a) ACZnS-220-5wt% (b) ACZn-200-50wt% and ACZnS-200-50wt%



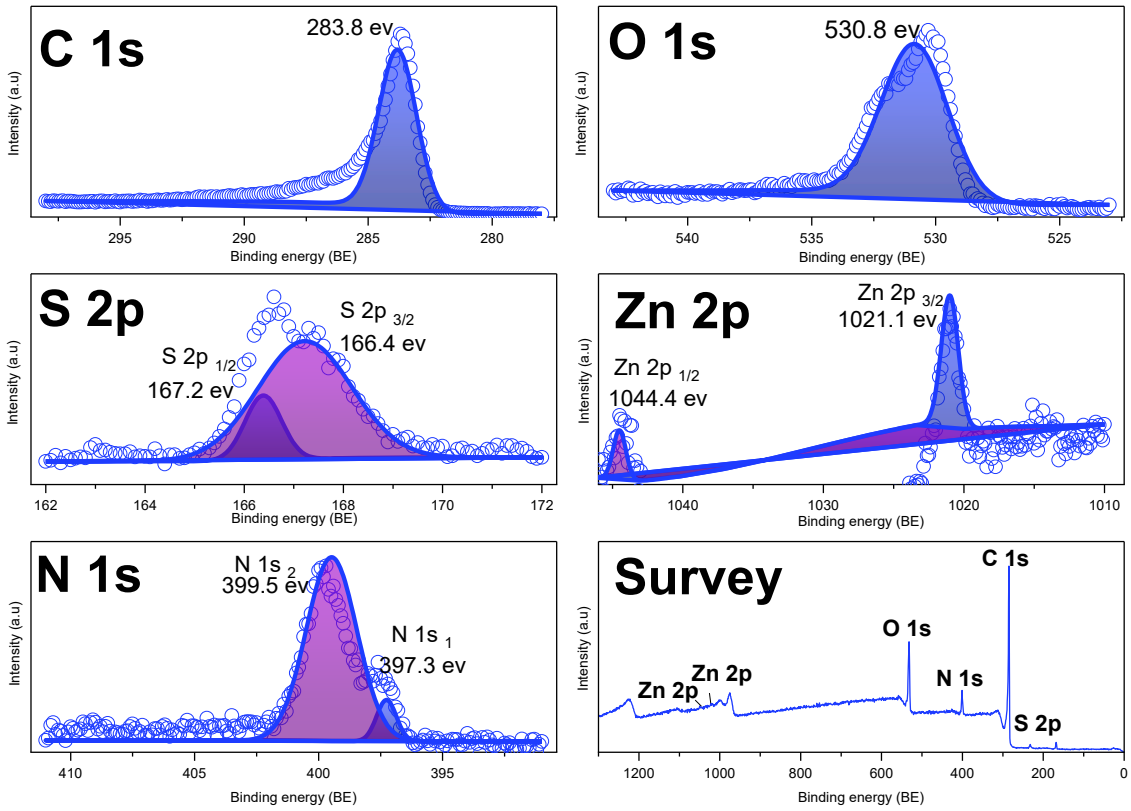
Figure S3. FTIR analysis ACZnS-220-5wt%

Table S1. EDX analysis of ACZnS-220-5wt%

Element	SEM Analysis ACZnS-220-5wt% spots (wt%)							Average (wt%)
	1	2	3	4	5	6	7	
Carbon	77.44	75.95	74.42	75.95	78.64	69.71	61.26	73.34±5.59
Oxygen	18.47	8.23	22.17	14.21	9.42	4.65	4.14	11.61±6.39
Aluminum	0.06	0.01	0.01	0.03	0.16	-	0.26	0.08±0.09
Silicone	0.17	0.04	0.08	0.51	0.19	1.27	1.51	0.54±0.56
Sulphur	2.25	7.38	1.93	7.71	6.61	17.09	29.27	10.32±9.02
Zinc	1.61	8.37	1.40	1.60	4.97	7.28	3.56	4.11±2.65

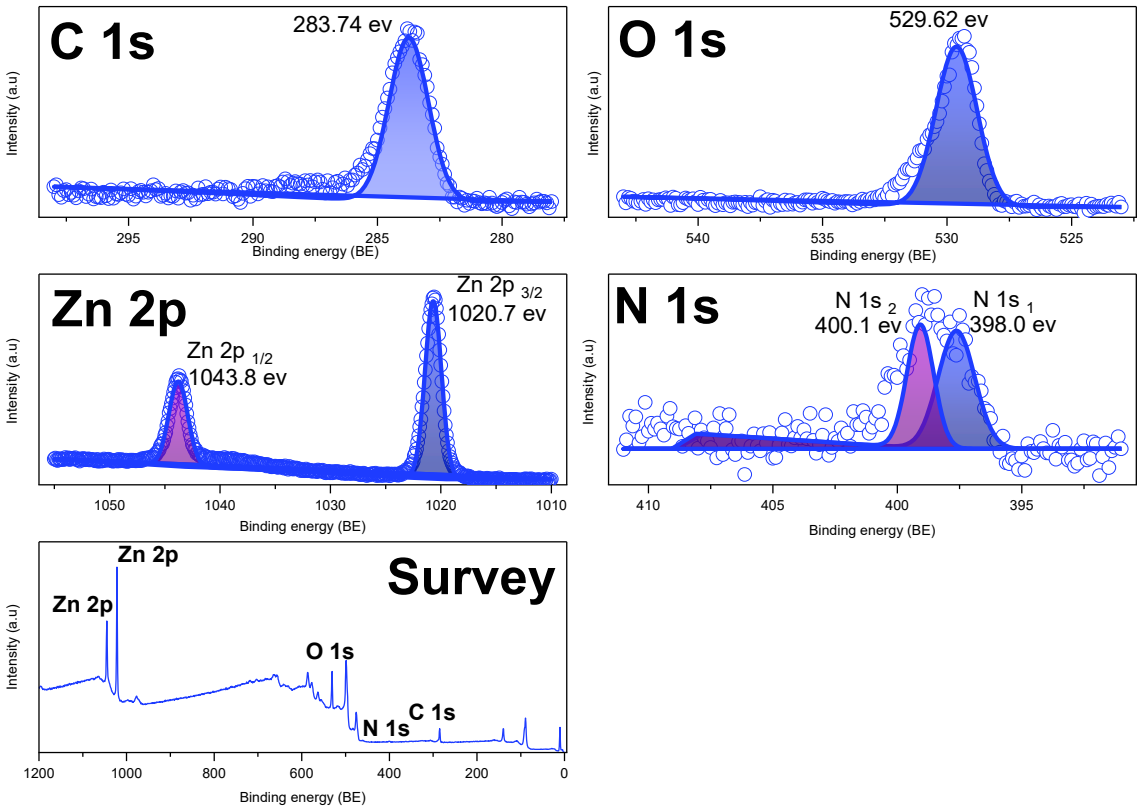
923

924



925

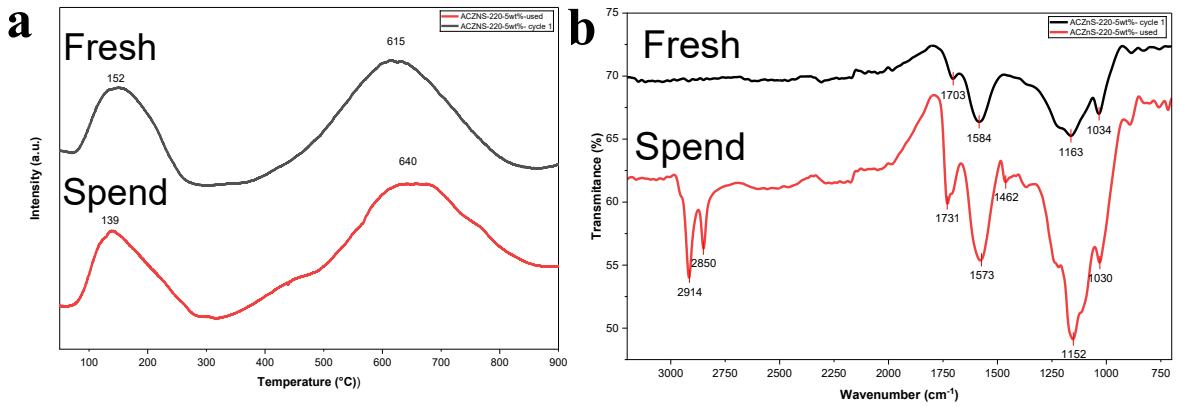
926 **Figure S4**. Deconvoluted XPS spectral peak in the C_{1s}, O_{1s}, Zn_{2p}, S_{2p} and N_{1s} structures
927 ACZnS-220-50wt%



928

929 **Figure S5**. Deconvoluted XPS spectral peak in the C1s, O1s, Zn2p, and N1s structures ACZn-

930 220-50wt%



931

932 **Figures S6.** (a) TPD-NH_3 analysis for ACZnS-220-5wt%-cycle 1 and ACZnS-220-5wt%-used

933 (b) FTIR analysis for ACZnS-220-5wt%-cycle 1 and ACZnS-220-5wt%-used

934

935

Table S3. TPD-NH_3 analysis of fresh and spend catalyst

Catalyst	Acidity (μmol/g)	Total (μmol/g)
ACZnS-220-5wt%-	152	480.93
Fresh	615	3374.36
ACZnS-220-5wt%-	139	970.59
Spend	640	2217.31